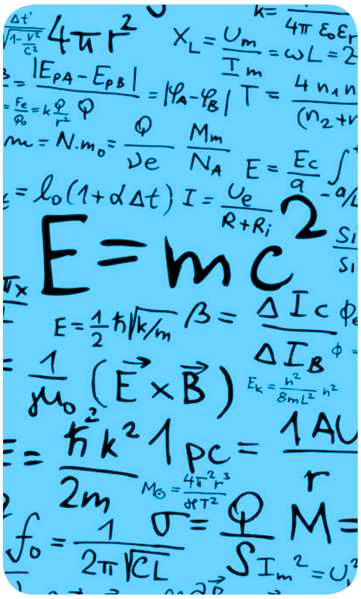

MÁSTERES de la UAM

Facultad de Ciencias /11-12

Máster en Química Teórica y Modelización Computacional

UNIVERSIDAD AUTONOMA DE MADRID

Campus Internacional excelencia UAM CSIC+

Vibrational deexcitation and rotational excitation $H_2(D_2)/Cu(111)$: adiabatic vs nonadiabatic

Alberto Pablo Sánchez Muzas

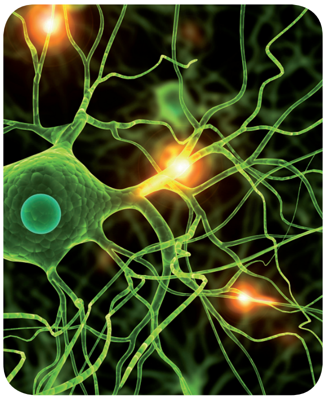

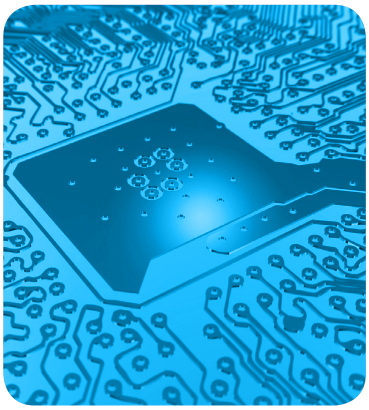

UAM EDICIONES

MASTER IN THEORETICAL CHEMISTRY
AND COMPUTATIONAL MODELLING

Vibrational deexcitation and rotational excitation of H_2 and D_2 scattered from Cu(111): Adiabatic versus non-adiabatic dynamics

Author:
Alberto Pablo Sánchez Muzas

Supervisor:
Dr. Cristina Díaz

Departamento de Química
Facultad de Ciencias
Universidad Autónoma de Madrid (Madrid, Spain)

July 13, 2012

Acknowledges

- I would like to thanks, first of all, Prof. Fernando Martín for giving me the possibility of working in one of his research projects in the Universidad Autónoma de Madrid, and Dr. Cristina Díaz, my advisor, who followed me with constancy during the entire master thesis project. I would like to thanks as well Prof. Geert-Jan Kroes and the entire theoretical group in Leiden Institute of Chemistry for their kindness when I was staying in Holland and their patience teaching me how to introduce temperature effects in molecule-surface simulations, I really felt like a part of the group. I am also very grateful to the Centro de Computación Científica from Universidad Autónoma de Madrid, who provided us with all the computational power we needed for the calculations done in this work. Last but not least, I would like to thank my parents and all my family, without whose support nothing of this would have been possible, specially my young sister Andrea, who has livened up my tedious moments.

- Me gustaría das las gracias, en primer lugar, al Prof. Fernando Martín por darme la posibilidad de trabajar en uno de sus proyectos de investigación en la Universidad Autónoma de Madrid, y a la Dra. Cristina Díaz, mi supervisora, quien me ha seguido con constancia durante todo el presente proyecto. Me gustaría también agradecer al Prof. Geert-Jan Kroes y al grupo completo de química teórica del Leiden Institute of Chemistry por su amabilidad durante mi estancia en Holanda y paciencia al enseñarme cómo introducir los efectos de la temperatura en simulaciones molécula-superficie. Realmente me sentí uno más del grupo. Estoy también agradecido al Centro de Computación Científica de la Universidad Autónoma de Madrid por garantizarnos los recursos computacionales que nuestros cálculos requerían de una manera eficiente. Por último, pero no menos importante, me gustaría dar las gracias a mis padres y familiares, sin cuyo soporte nada de esto habría sido posible, especialmente a mi hermana menor Andrea, quien me amenizó en mis momentos más tediosos. Gracias a todos.

Contents

CHAPTER 1

Introduction

SECTION: 1.1

Surface science

The growth and refinement of new technologies demands each day a better knowledge of how atoms and molecules interact on different material surfaces. Some particular applications in which surface science plays a major role are, among others, the *heterogeneous catalysis*, fundamental for most of the usual industrial synthetic processes[1–3]; the development of *new surface characterization techniques,* as the recent discovery of fast atom diffraction at grazing angle[4]; the simulation of *corrosion* processes; the development of new *hydrogen containers*[5;6]; or the simulation of *self-organization processes* on particular surfaces [7], interesting for the improvement of nano-electronic devices. These examples can give us an idea of the richness that can be extracted from surface science in order to make easier our diary life. But probably, despite the wide range of open branches that have been favored in the recent years, heterogeneous catalysis is the most known and recognized area in which this science is contributing. In fact, one of the achievements recognized by the 2007 Nobel Prize in Chemistry, awarded to Gerhard Ertl, was the detailed description of the sequence of elementary reactions that takes place during the Haber process[8], fundamental for low cost ammonia production, in which molecule-surface interactions plays a major role. Therefore, we will focus on heterogeneous catalysis.

Heterogeneous catalysis is really interesting to the majority of industrial chemical processes. Most of the products that are massively synthesized are liquids or gases so that the use of a solid catalyst is convenient (easy to separate and re-use). In fact, the 90% of chemical manufacturing processes employ solid catalysts[9] at least in one of their production steps. Some common examples are, among others: the NH_3 synthesis from nitrogen and hydrogen molecules (Haber process), which is a key product to the production of fertilizers; methanol synthesis from CO and H_2, used as a solvent; ethylene oxidation, interesting to antifreeze industry; hydrogenation of vegetable oils to produce margarine; or nitric acid synthesis from NH_3 oxidation. In general, the vast majority of solid catalyst are based on metals (Pd, Pt, Cu, Au, ...) or metal-oxides (MgO, ...), thus, we can find a large amount of studies focused in these kind of surfaces in the literature.

In a typical heterogeneous catalysis scheme, chemical reactions take place on the solid catalyst surface, where the well-ordered bulk structure is truncated. The interaction of a molecule with this semi-infinite surface is more complex than the usual molecule-molecule interaction in a pure gas phase framework. There is a large number of physical conditions that can influence the reaction path, for instance, the surface temperature (molecule-phonon interaction), electron-hole pair excitations, the presence of impurities adsorbed on the surface (difficult to control experimentally), the presence of local defects, the surface coverage, the energy available to the impinging molecule (energy exchange between molecular degrees of freedom), etc. Thus, it is needed a dynamical approach to catch the essential physics of the problem. Despite the great computational power available for theoretical calculations, a "complete" quantum modelling of the dynamics of gas/surface interactions at experimental conditions cannot be achieved in most cases and several approximations have to be taken.

In order to achieve reliable conclusions in surface science, we need both theoretical and experimental information. From the point of view of a theorist, it is difficult to obtain accurate results without any previous knowledge of the system that it is being simulated, specially if the surface structure is not known. Calculations in surface science are usually time-consuming and a lot of ideal approximations should be taken. Hence, comparison with experiment always helps surface scientists to sharpen the theoretical tools available in order to get a good compromise between accuracy and time expense. From the point of view of an experimentalist, it is difficult to know what is happening at the atomic scale level without any theoretical guidance. Sometimes experimental models are too simplistic and theoretical treatments can provide a good way to improve future measurements. As a result, surface science is a perfect environment to theory-experiment collaboration.

SECTION: 1.2

Molecules interaction with surfaces

In this section, we focus on the interaction of diatomic molecules with a frozen metal surface. A good qualitative knowledge of this, in principle, simple system is necessary to understand the basic physics that underlies more complex processes on metal surfaces. We can divide molecule-surface processes in three big groups:

I) Molecular adsorption: a molecule coming from the vacuum transfers its momentum to the lattice, such that it equilibrates with the surface and is stuck on it. There are three possible mechanisms for a diatomic molecule to be stuck on a surface:

1. *Dissociative chemisorption mechanism* (Fig. 1.2.1)*:* the impinging molecule relaxes its internal bond as it approaches to the surface due to the individual atom-surface interaction. Finally, the bond is broken and the individual atoms are adsorbed on the surface.

2. *Molecule-surface adsorption mechanism* (Fig. 1.2.2)*:* the impinging molecule coming from the vacuum is chemisorbed or physisorbed on the surface, but remains intact.

3. *Abstraction mechanism* (Fig. 1.2.3)*:* similar to the previous mechanism but only one atom remain on the surface. The other atom is scattered back to the vacuum.

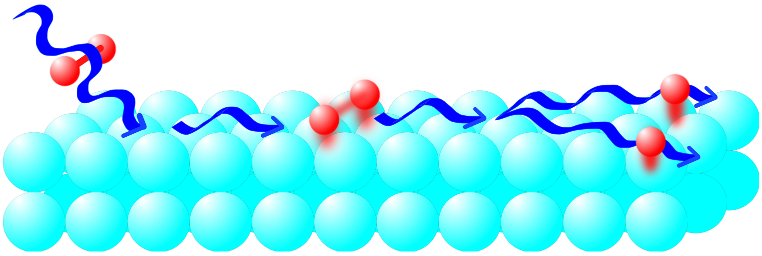

Figure 1.2.1: Dissociative chemisorption mechanism.

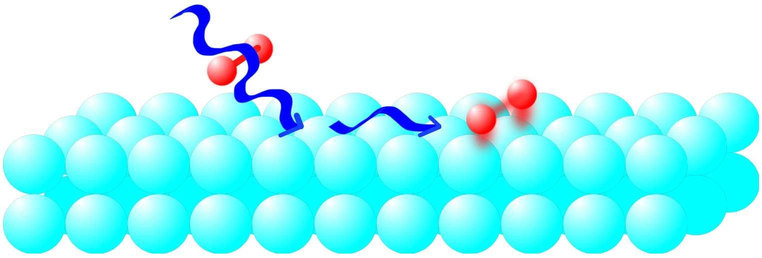

Figure 1.2.2: Molecule-surface adsorption mechanism.

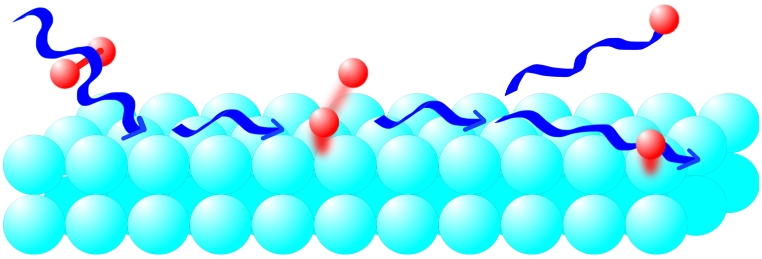

Figure 1.2.3: Abstraction mechanism.

II) Molecular desorption: it is the opposite process of molecular adsoption, i.e. a molecule/atom already adsorbed on the surface is released to the vacuum. There are three possible mechanisms:

1. *Langmuir-Hinshelwood mechanism:* atoms/molecules already adsorbed and thermally equilibrated with the surface spend a time traveling on the surface and later collide in such a way that a new molecule is generated and scattered back to the vacuum. Reverse process of dissociative chemisorption mechanism.

2. *Eley-Rideal mechanism:* an atom coming from the vacuum collide with an atom adsorbed on the surface. An inmediate reaction takes place and a molecule (the product) is scattered back to the vacuum. Reverse process of abstraction mechanism.

3. *Hot-atom mechanism:* an atom adsorbed on the surface in equilibrium with it reacts with another atom that has recently arrived from the gas phase (not equilibrated yet).

Experimental data regarding reaction probabilities are usually measured from molecular desorption processes assuming detailed balance, which means that at equilibrium, molecular desorption and adsorption rates should be equal (they are microreversible processes). This way, the properties of reacting molecules can be measured closer to the reaction barrier.

III) Molecular scattering: a molecule coming from the vacuum is reflected by the repulsive force generated by the surface at short distances (Fig. 1.2.4). During this process, molecular degrees of freedom (DOFs) can exchange energy between them or with the surface. Thus, the final state of the molecule, can change respect to the initial one. In a frozen surface scheme, the energy exchange can be only produced via molecular DOFs coupling favored by the surface or electron-hole pair excitations if we take into account non-adiabatic processes. There are four types of scattering for diatomic molecules:

1. *Elastic scattering:* there is not any transfer of energy. The initial and the final vibrational and rotational quantum states are equal.
2. *Vibrationally inelastic scattering:* only the vibrational quantum state changes with respect to the initial one.
3. *Rotationally inelastic scattering:* only the final rotational quantum state changes with respect to the initial one.
4. *Diffraction:* when a molecule is scattered from a periodic surface, the projectile parallele momentum to the surface plane can only change by discrete amounts. Diffraction is observed whenever the wavelength associated to the particle is of the order of the surface inter-atomic distance. This is a well-known quantum effect that makes the angular distribution of a molecular beam scattered from the surface to present a discrete peaks distribution.

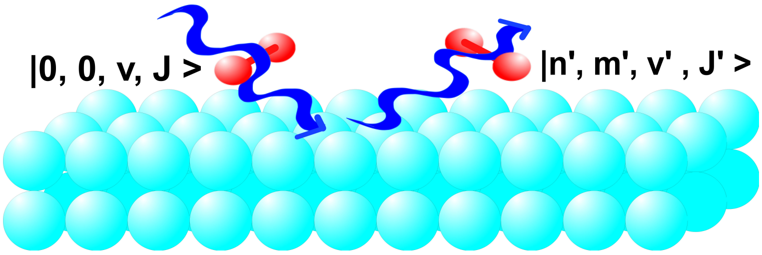

Figure 1.2.4: A general scattering scheme. (v) is the vibrational quantum number, (J) the rotational quantum number, and (n,m) the diffraction numbers.

1.2.1

Activated and non-activated systems

We can think in a dissociative reaction mechanism similarly to a simple gas phase reaction in which there is a reaction path that connects the reactants (isolated molecule) with the products (adsorbed atoms) going through a reaction barrier that dominates the kinetics of the process. With this simplistic picture in mind, we can understand the two basic dissociation (reflection) probability profiles (plotted as a function of the incidence energy) that a molecule-surface system can present:

I) Activated systems: the dissociation (reflection) probability increases (decreases) monotonically with the incidence energy and it is close to zero (one) for very low energies. This systems are characterized by an early barrier (close to the reactants zone) or a late barrier (close to the products zone, closer to the surface) that cannot be overcome until the available energy of the impinging molecule is sufficiently high. A molecule that encounters a too high reaction barrier in its path toward the surface is reflected to the vacuum. Of course, if the molecules are light, tunneling effects can contribute to high the reaction probabilities at low incidence energies. Some examples of activated systems are H_2/Cu[10], H_2/Ag(111)[11], D_2/Ag(100)[12] or H_2/Ni(111)[13].

II) Non-activated systems: the dissociation (reflection) probability presents a non-monotonous behavior as a function of the incidence energy. First, the reaction probability (reflection) decreases (increases) with the incidence energy, but later, a minimum (maximum) value is reached after which the reaction (reflection) probability increases (decreases) with the incidence energy. In this kind of systems, there are reactive channels that do not present a reaction barrier. Thus, the reaction probability at low incidence energy is not close to zero but to one. The are several mechanism that have been proposed to explain the shape of the reaction probability as a function of E_i: the steering effect or the dynamic trapping combined with direct dissociation.

1. *Steering effect*[14]: at low incidence energy, the impinging molecule has such a slow velocity that it has time to orient and travel across barrierless paths of the potential energy surface (if we keep the adiabatic picture in mind). When the molecular translational energy increases, the molecule orientation decrease (less time to rotate) and the reaction probability is lowered. At high incidence energy, activated channels can also be overcome enhancing reactivity again.

2. *Dynamic trapping and direct dissociation:* dynamic trapping is a process in which an impinging molecule/atom rebound several times on the surface (do not need to exchange energy with the surface) so that it looses its initial incidence angle “memory”. This effect is only efficient at low energies and can be followed by a dissociative adsorption reaction. Molecules that react in this way give rise to the concept of indirect reaction which scales with the total incidence energy and not with the normal energy like the direct dissociation (the reaction takes place just after the molecule collides with the surface). Both types of reactions occurs in a non-activated system. It have been shown that the competition between them can explain the non monotonous reaction probability profile of non-activated systems, such as, for example, H_2/Pd(111)[15].

   Some examples of non-activated systems are: H_2/Pd(100)[16], H_2/Pd(110)[17], H_2/Pd(111)[18], H_2/W(100)[19] or H_2/Ni(110) and H_2/Ni(100)[20].

SECTION: 1.3

H_2/D_2+ metal surface system: background

The simplicity of H_2/metal system, makes it a perfect prototype to study gas/metal surface interactions. It has been treated in a wide number of either experimental or theoretical investigations. Theoretically, H_2/metal is one of the most simple models that a surface scientist can think about. The reason of this is twofold:

- Theoretical and experimental work has shown that phonons do not affect the reaction in a major way. Also, it is usually assumed that electron-hole pair excitations do not affect the reaction essentially. This means that the reaction process can be treated in the static surface Born-Oppenheimer approximation framework (see section 2.1).

- We can treat its molecular DOFs (nuclear and electronic) quantum mechanically with essentially no approximations because hydrogen atoms are light.

1.3.1

Theoretical background

The first quantum calculations simulating the dynamics of dissociative adsorption on a molecule-surface system, were carried out for the non-activated system H_2/Ni(100)[21]. Due to the high computational cost involved, it was only taken into account two dimensions, namely, the interatomic (r) and the molecule-surface (z) distance. Later, a similar study was carried out for the H_2/Cu(100) system[22].

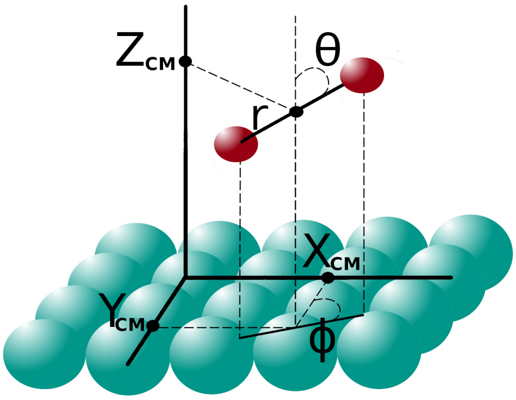

Figure 1.3.1: Hydrogen molecular degrees of freedom.

With the improvement of available computational power and refinement of theory, further better low dimensional treatments were published years later. In the case of three-dimensional studies, we can find, for example, those made for the H_2/Ni(100)[23], $H_2(D_2)$/Ni(100)[24] and H_2/Cu[25;26] systems taking into account (z), (r) and the rotational polar angle (θ) DOFs; and those made for H_2/Cu(111) and H_2/Pd(100)[27] including the minimun energy path (s), (r) and the translational movement projected on the (x) direction, defined as the line that links the first neighbors in the surface. In the case of four-dimensional studies, we can highlight, among others, those made for the H_2/Cu system studying the dependence of the dynamics for different sets of DOFs like (r, z, θ, ϕ)[28;29] or (r, z, x, y)[30], being (ϕ) the molecular azimuthal angle and (y) the direction perpendicular to (x).

The first quantum studies that included all the molecular DOFs, i.e. 6D calculations, were carried out by Groß *et al.*[14] in order to study the non-activated system H_2/Pd(100). In the case of activated systems, the first 6D quantum calculations were done for H_2/Cu(111)[31] and H_2/Cu(100)[32;33]. In these studies, it was found that reaction barriers can depend strongly on the impact site (it can vary in 0.90 eV) and also on the orientation of the impinging molecules respect to the surface (reaction of only nearly helicopter-like impinging molecules, hindered orientations, etc.). An exhaustive compilation of the findings achieved by these studies is given in Refs. [34]. The main idea that high dimensional simulations give rise is that all the molecular DOFs can affect strongly the dynamics of molecule-surface systems. They cannot be neglected or averaged if we want to model accurately the reaction barriers that molecules encounter in their pathway upon the surface. This is not possible for heavier molecules as O_2, CO or NO where quantum calculations are more complicated (e. g. more electronic DOFs, stronger molecule-phonon interaction, etc.) and time demanding. To treat them, it is promising the use of classical dynamics.

Classical and quasi-classical (classical + ZPE[1]) calculations were applied for molecule-surface problems in the later '90s. We can fin in the literature comparative studies between classical and quantum results that, in general, yield to reasonable agreements. In order to cite some of them, we can remark those done for H_2/Cu(111), H_2/Cu(110), H_2/Ni(111) and H_2/Ni(110) systems by Engdahl *et al.*[34;35] and for H_2/Pd(100) system by Groß *et al.*[36]. From the literature, it is also clear that pure classical dynamics suits better for non-activated systems whereas quasi classical calculations reproduce better activated systems, where the available ZPE is crucial for a correct description of the reactivity. Nevertheless, both approximations can be explicitly corrected to treat any system[37].

1.3.2

Experimental background

H_2/Cu system has been experimentally the first and most studied system in surface science. There has been a vast amount of experimental studies of H_2 interacting with metal surfaces, therefore only a few experiments will be mentioned in this section. Later, in section 1.4 we will discuss some experiments that give evidences of the failure of the adiabatic approach, which is the main topic of the present work. Now, we will only focus on a general classification of experimental methodologies. More information about the study of H_2 interacting with metal surfaces is provided in Ref. [38].

We can classify experimental methodologies into two big groups:

I) Molecular beam diffraction: in this kind of experiments, a molecular beam collides with a surface and is partially reflected. There are several parameters that can be selected for the initial conditions, e.g. the incidence angle, the incidence energy or the rovibrational quantum state population. There are several techniques to analyze the outcoming beams. The commonest ones are the angular distribution and the time-of-flight (TOF[39]) measurements, which allow us to calculate the molecules translational energy variation; and the REMPI[2] technique, which is used to determine the rovibrational state of the outcoming molecules. Usually, this methodology is applied for activated systems because, otherwise, in non-activated systems, the dissociative reaction probability is so high that it is difficult to detect the scattered molecules. Some examples of experimental studies for activated systems are: H_2/Cu(100)[40], D_2/Cu(111)[41;42] or HD/Ag(111)[43]. In the case of non-activated systems we can highlight: D_2/Rh(110)[44] or H_2/Pd(111)[45] among other studies.

In these experiments, it is obtained relative intensity peaks. The detectors measure the rate of molecules that are arriving per unit time. In order to compare with theoretical results, it is necessary to calculate the absolute probabilities. A way to do that is calculating the total reflectivity as:

$$R_G = \frac{\sum\limits_{J_i,J_f} I_G^{J_i,J_f}}{I_i} \tag{1.3.1}$$

where I_i is the incident beam intensity and $I_G^{J_i,J_f}$ the intensity of each individual diffraction peak. With similar expressions, we can calculate absolute probabilities for the individual peaks.

The development of new experimental selective techniques as the stimulated Raman pumping (SRP, do not confuse it with the specific reaction parameter approximation that will be mentioned later in chapter 2) combined with the REMPI, has allowed surface scientists to carry out state-to-state

---

[1] Zero point energy.

[2] Resonance enhanced multiphoton ionization.

resolved scattering experiments. The former technique was designed to overpopulate specific rovibrational quantum states in the incident molecular beam, whereas with the latter we can measure the rovibrational channels in the outcoming one. As a result, it is possible to obtain experimental data about vibrational and rotational inelastic processes for an specific quantum state of the incident molecules. In this kind of experiments, TOF measurements are needed. Some interesting results that have been obtained applying these techniques in different systems are, among others:

- The rotational excitation for HD molecules is higher than for H_2 molecules.
- There is an important energy transfer from vibration to rotation in the H_2/Pd(111) system.
- The existence of an isotope effect in the $H_2(D_2)$/Cu(111) vibrational deexcitation probabilities. This will be discussed in sections 1.5 and 1.6, because it is important for the purpose of this work.

II) Adsoption (desorption) experiments: this kind of experiments can be divided also into two groups:

1. *Molecular beam techniques:* similar to molecular beam diffraction methods but focused on the measurement of sticking coefficients. One way to obtain the desired observables is to study the relation of the incident and outcoming beam intensities[46]. Another option is to study the number of molecules deposited on the surface (coverage index). In the latter experiments, the temperature programmed desorption (TPD) method[47] or the King and Wells technique[48] are used. There are a lot of systems in which theses techniques have been applied, and interesting results were obtained but we will only focus in those where the H_2/Cu system was involved:

   - Measurements of sticking coefficients in H_2/Cu(111), Cu(100) and Cu(310) systems[49] as a function of the incidence angle θ_i showed that the dissociative adsorption in these systems depends only on the normal incidence energy (lack of corrugation).
   - It was first found that the dissociative adsorption probability in H_2/Cu(110)[50] system increases with the vibrational energy available for the impinging molecules.
   - For the H_2Cu/(111)[51] system, it was shown that the dissociation probability decreases when the initial rotational quantum number (J_i) increases for low values of J_i ($J_i \leq 6$). However, if $J_i > 6$, dissociation probability increases with J_i. The same effect was found in H_2/Pd(111)[45] system for $J_i \leq 4$.

2. *Permeation method*[52]: in this method, molecules are injected to one face of the sample plate (typically with a thickness between 0.5 and 1.0 mm). On this plate, molecules dissociate and go through the opposite face, where they react and form new molecules. These molecules are then scattered back to the vacuum. The plate where the molecules are injected is maintained at 1000 K and 1 bar of pressure. The main idea underlying this apparatus is the microreversibility principle, which connects the associative desorption with the opposite phenomenon, the dissociative adsorption. Some systems in which this method have been applied successfully are H_2/Cu(110) and H_2/Cu(111)[53;54].

SECTION: 1.4

Failure of the adiabatic approximation

The existence of electronic excitations during the interaction of diatomic molecules with surfaces cannot be negated. Experimental studies carried out in the last four decades, have succeed to detect an increasing quantity of molecule-surface phenomena that cannot be simulated within the adiabatic approximation (see section 2.1). These studies have provided a great source of detailed information to contrast state-of-the-art theoretical treatments and to reopen the main question of whether the Born-Oppenheimer approximation (BOA) can accurately describe gas-surface reactions or not.

The BOA is usually the main approximation in theoretical chemistry. However, there are good reasons to think that breakdowns of the BOA will be even more probable in chemical processes taking place on metal surfaces than in a pure gas phase scheme:

1. Surfaces can stabilize polarizable excited electronic states so that they get closer to the ground state, increasing the probability of electronic transitions. This effect if stronger in charged molecules.
2. Low work function metals have their surface electrons attached weakly compared to the common value of molecular and atomic ionization potentials.
3. Electronic states forming the conduction band of the metal are not separated energetically. They form a continuum of states which provides an effective mechanism for energy exchange with molecular DOF.
4. Large-amplitude vibrational motion of reacting molecules approaching to a reaction barrier can yield to severe electronic reorganization processes. For the same reason, high vibrationally excited molecules are expected to interact non-adiabatically with surfaces.

The first evidence of the BOA breakdown for adsorbates at metal surfaces was found in the comparative study of the infrared spectra of isolated and adsorbed CO molecules. It was discovered that the C-O stretching mode signal broadens due to the coupling of M-CO bond (where M is a metal) and C-O motion. The mechanism involved is well-known[55;56]: there is a charge transfer from the metal to the CO π^* antibonding orbital (backbonding) that increases the amplitude of the C-O motion (the bond is weaken). More recent evidences of BOA breakdown can be found in NO/Ag(111) scattering experiments[57;58]. In this studies, vibrational de-excitation probabilities NO($v=2\rightarrow 1$) were measured. The results showed a strong dependence of vibrational de-excitation on the incidence energy which is a behavior typically related with an energy exchange between the molecular vibration and the electronic DOF of the surface[59;60]. There have been also measurements of chemicurrents and creation of hot electrons during the chemisorption of atoms and molecules on metal films surfaces[61–63].

The adsorption of O_2 on Al (111)[64] and Ag(100)[65] is a conspicuous example of failure of the BOA. Adiabatic calculations[66] predict a barrierless dissociative reaction process while in the experiment it is found a reaction probability profile typical for an activated system. However, in the same reference, qualitative agreement with the sticking curve is reached with classical dynamics forcing the impinging O_2 molecules to remain their excited spin-triplet state. Theoretical calculations[67;68] have been also able to mimic multi-quantum vibrational relaxation of NO molecules scattered from Au(111) with electron hoping methods. More recently, low dimensional calculations performed in Ref. [69] suggest that electronic friction models can reproduce most of the results obtained in this kind of experiments.

So far, we have discussed some representative molecule-surface systems in which it is known how the non-adiabatic interaction rise. However, electron-hole (e-h) pair excitations are still controversial for closed-shell molecules, which are initially in their ground state. In the case of N_2/Ru(0001) system[70], low-dimensional non-adiabatic dynamics based on friction coefficient methods (see sec. 2.4) suggests that the huge discrepancies between low-dimensional adiabatic calculations and the experiment were mostly due to e-h pair excitations. But, 6D adiabatic calculations[71] have shown that most of the discrepancy found between theoretical and experimental results in this system vanishes when all the molecular DOFs are included in the simulation. In fact, six dimensional simulations within the BOA have succeed mimicking H_2/Pt(111)[72] non-reactive scattering and N_2/W(110)[73] rotational state distribution in scattering experiments. High-dimensional DFT-LDA[3] based calculations including non-adiabatic effects via friction coefficients have also shown that e-h pair excitations do not play a major role in the dynamics of H_2/Cu(110) and N_2/W[74] dissociative adsorption or in the scattering of N_2 on W(110) and N from Ag(111)[75].

SECTION: 1.5

Master thesis motivation: objectives

Adiabatic simulation of H_2 interacting with copper surfaces have shown to be in good agreement with experiment[31;40;76–79]. In fact, in Refs. [78;79] a new DFT exchange-correlation functional was developed and adapted to H_2/Cu(111) system within the BOSS[4] approximation that yielded to quantitative agreement with a wide variety of experiments (e.g. dependence of reaction on incidence energy and rovibrational initial state or rotationally inelastic scattering). Despite this agreement, it has been suggested[80] that e-h pair excitation could play a major role in H_2/Cu(100)[40] and D_2/Cu(100)[41] vibrationally inelastic scattering process, where experimental evidence of isotope effects have been found. Theoretical results obtained by a low dimensional non-adiabatic calculation using friction coefficients[80], similar to the one used in Ref. [70] for N_2/Ru(0001) system, seems to support that idea. However, as we have seen in the previous section, there are good reasons to think that a 6D adiabatic treatment could be enough to reproduce the experimental findings.

The main goal of this work is to elucidate if six dimensional quasi-classical dynamics within the BOSS approximation scheme can give an explanation of the isotope effect found in Refs. [40;41]. In order to achieve this aim, we will use in our calculations three different potential energy surfaces[78;79] obtained by DFT-GGA[5] *ab initio* calculations for the $H_2(D_2)$/Cu(111) system. We will carry out also 6D non-adiabatic friction based calculations. From the comparison of both approaches we will be able to estimate the impact of electron-hole pair excitation on the dynamics of $H_2(D_2)$/Cu(111) system.

This work is organized in the following two chapters:

- **Chapter 2 - Theory:** in this chapter, we will show the theoretical tools that we have used in our calculations. First, we will describe the implications of the Born-Oppenheimer static surface approximation. Later, we will explain roughly how the potential energy surfaces were obtained. Finally, we will present a discussion on adiabatic dynamics methods (quasi-classical and quantum mechanical) and non-adiabatic dynamics based on the local friction approximation.

---

[3] Density functional theory - local density approximation.

[4] Born-Oppenheimer static surface

[5] Density functional theory - generalized gradient approximation.

- **Chapter 3 - Results:** in this chapter, we will show all our results organized into 5 different sections. The first two sections are dedicated to introduce the reader to the isotopic effect found in the experiments for H_2/Cu(100)[40] and D_2/Cu(100)[41] systems and the low-dimensional non-adiabatic dynamics results obtained by Luntz et al.[80]. The next two section are dedicated to the exposition of our theoretical results. The last section contains a brief summary of the conclusions obtained.

CHAPTER 2

Theory

The scattering of molecular hydrogen from a crystal surface is, in principle, one of the simplest molecule-surface problems that a surface scientist can face. However, deriving *ab initio* theoretical treatments that yield to an accurate dynamical description of this system is not a trivial task at all. In this chapter, we will provide a discussion of the theoretical methods and approximations that have been made in this work.

SECTION: 2.1

Born-Oppenheimer static-surface (BOSS) approximation

The Born-Oppenheimer approximation (BOA) assumes that electrons move much faster than nuclei (due to the mass missmatch), and therefore, that electrons can adapt instantaneously to a differential movement of the nuclei, i.e. electrons follow the motion of the nuclei adiabatically.

Let us consider a system of N nuclei described by generalized spatial coordinates $\boldsymbol{Q} = (\boldsymbol{Q}_1, \boldsymbol{Q}_2, \dots, \boldsymbol{Q}_N)$ and conjugated momenta $\boldsymbol{P} = (\boldsymbol{P}_1, \boldsymbol{P}_2, \dots, \boldsymbol{P}_N)$; and N_e electrons described by generalized spatial coordinates $\boldsymbol{q} = (\boldsymbol{q}_1, \boldsymbol{q}_2, \dots, \boldsymbol{q}_{N_e})$ and conjugated momenta $\boldsymbol{p} = (\boldsymbol{p}_1, \boldsymbol{p}_2, \dots, \boldsymbol{p}_{N_e})$, where $\boldsymbol{Q}_i, \boldsymbol{P}_i \in \mathbb{R}^3$ and $\boldsymbol{q}_i, \boldsymbol{p}_i \in \mathbb{R}^3$. The non-relativistic and non-magnetic Hamiltonian that describes the physics of the problem takes the form:

$$H(\boldsymbol{Q}, \boldsymbol{P}, \boldsymbol{q}, \boldsymbol{p}) = T_n(\boldsymbol{P}) + T_e(\boldsymbol{p}) + V_{n-e}(\boldsymbol{Q}, \boldsymbol{q}) + V_{e-e}(\boldsymbol{q}) + V_{n-n}(\boldsymbol{Q}) \tag{2.1.1}$$

where T_n , T_e are the kinetical energy terms for the nuclei and electrons respectively, and V_{n-e}, V_{n-n}, V_{e-e} are the coulomb interaction terms nuclei-electrons, nuclei-nuclei and electrons-electrons respectively. As the Hamiltonian does not depend explicitly on time, the time-dependent Schrödinger equation leads to the well known eigenvalue problem:

$$i\hbar \frac{\partial}{\partial t} \Psi(\boldsymbol{Q}, \boldsymbol{q}, t) = \hat{H} \Psi(\boldsymbol{Q}, \boldsymbol{q}, t) \Rightarrow \boxed{\hat{H} \psi(\boldsymbol{Q}, \boldsymbol{q}) = E \psi(\boldsymbol{Q}, \boldsymbol{q}); \quad \Psi(\boldsymbol{Q}, \boldsymbol{q}, t) = \psi(\boldsymbol{Q}, \boldsymbol{q}) e^{\frac{-iEt}{\hbar}}} \tag{2.1.2}$$

Although Eq. 2.1.2 depends on nuclear and electronic coordinates, within the BOA it only depends parametrically on nuclear coordinates (denoted with an upper tilde $\widetilde{\boldsymbol{Q}}$). Thus, the wave function $\psi(\widetilde{\boldsymbol{Q}},\boldsymbol{q})$ can be separated into an electronic $\phi(\widetilde{\boldsymbol{Q}},\boldsymbol{q})$ and a nuclear $\chi(\widetilde{\boldsymbol{Q}})$ part, which is possible only if the gradient of $\phi(\widetilde{\boldsymbol{Q}},\boldsymbol{q})$ respect to nuclear coordinates is negligible ($\vec{\nabla}_{\boldsymbol{Q}}\phi(\widetilde{\boldsymbol{Q}},\boldsymbol{q}) \approx \boldsymbol{0}$). This leads to the following equations of motion:

$$if\ \psi(\widetilde{\boldsymbol{Q}},\boldsymbol{q}) = \phi(\widetilde{\boldsymbol{Q}},\boldsymbol{q})\chi(\widetilde{\boldsymbol{Q}})\ and\ \vec{\nabla}_{\boldsymbol{Q}}\phi(\widetilde{\boldsymbol{Q}},\boldsymbol{q}) \approx \boldsymbol{0}\ \Rightarrow \begin{cases} (1)\ \ \hat{H}_e\phi(\widetilde{\boldsymbol{Q}},\boldsymbol{q}) = \epsilon(\widetilde{\boldsymbol{Q}})\phi(\widetilde{\boldsymbol{Q}},\boldsymbol{q}); & \hat{H}_e = \hat{T}_e + V_{e-e} + V_{n-e} \\ (2)\ \ \hat{H}_n\chi(\widetilde{\boldsymbol{Q}}) = E\chi(\widetilde{\boldsymbol{Q}}); & \hat{H}_n = \hat{T}_n + V_{n-n} + \epsilon(\widetilde{\boldsymbol{Q}}) \end{cases} \tag{2.1.3}$$

For each $\widetilde{\boldsymbol{Q}}$ configuration, we obtain a set of $\{\phi_i(\widetilde{\boldsymbol{Q}},\boldsymbol{q})\}_i$ electronic eigenfunctions and a set of $\{\epsilon_i(\widetilde{\boldsymbol{Q}})\}_i$ electronic eigenvalues. The collection of all the i-esim enegy levels sampled for different spatial conformations $\widetilde{\boldsymbol{Q}}$ forms a potential energy surface (PES) $\{\epsilon_i(\widetilde{\boldsymbol{Q}})\}$. As Eq. 2.1.3(1) depends on all the electronic degrees of freedom, then it is prohibitive to solve it for a molecule-surface problem. Hence, we are forced to use the density functional theory (DFT) formalism instead of the usual orbital-wave function scheme to solve the problem. In section 2.2, we will discuss how the PES was calculated for this work.

Once we have a suitable PES, nuclear motion can be solved within a time-dependent quantum formalism:

$$i\hbar\frac{\partial}{\partial t}X(\boldsymbol{Q},t) = \left[\hat{T}_n + V_{n-n} + \epsilon_i(\boldsymbol{Q})\right]X(\boldsymbol{Q},t) \tag{2.1.4}$$

or using the Hamilton classical equations of motion:

$$H(\boldsymbol{P},\boldsymbol{Q}) = T_n(\boldsymbol{P}) + V_{n-n}(\boldsymbol{Q}) + \epsilon_i(\boldsymbol{Q})\ \Rightarrow \begin{cases} -\frac{\partial H}{\partial \boldsymbol{Q}_j} = \frac{d}{dt}\boldsymbol{P}_j \\ \frac{\partial H}{\partial \mathbf{P}_j} = \frac{d}{dt}\boldsymbol{Q}_j \end{cases} \tag{2.1.5}$$

Both ways to treat nuclear dynamics will be discussed in section 2.3.

So far we have not distinguish between molecular and surface nuclear coordinates. To take into account all molecular DOFs could make the system prohibitive even for DFT. In order to make the system treatable a static surface approximation is commonly used. Within this approximation, all the surface atoms are fixed to their equilibrium positions and their conjugated momenta are setted to $\boldsymbol{0}$. This yields to a drastic reduction of the DOFs of the system. In the case of an impinging diatomic molecule, like H_2 and D_2, we only have 6 DOF: 3 for its center of mass (X,Y,Z) and 3 for its internal motion, vibration (r) and rotation (θ, ϕ) (see Fig. 1.3.1). This approximation neglects the interaction and, therefore, the energy exchange, between the molecules and surface phonons, but, in the case of light molecules, such interactions are expected to be weak due to the large mass missmatch. Therefore, this approximation seems to be very reasonable specially for low surface temperatures.

SECTION: 2.2

Potential energy surface

2.2.1

Density functional theory formalism

DFT is based on the Hohenberg-Kohn theorems, which demonstrate that all the physical properties for a given system can be determined by simply knowing the density of its fundamental state $n_0(\boldsymbol{r})$. The main idea within this theory is that the energy can be written as a functional of the electronic density $E[n(\boldsymbol{r})]$, and therefore, that we are able to calculate $n_0(\boldsymbol{r})$ minimizing $E[n(\boldsymbol{r})]$ respect to $n(\boldsymbol{r})$. DFT is an exact theory of many-body systems but the exact expression of this functional is not known. In 1965, Kohn and Sham proposed to substitute the many-body problem by an auxiliary independent-particle problem so that the original electronic Schrödinger equation (Eq. 2.1.3(2)) is converted to N independent mono-electronic equations, which have the form:

$$\left\{-\frac{\hbar^2}{2m}\nabla^2 + v_{ext}(\boldsymbol{r}) + \int \frac{n(\boldsymbol{r}')}{|\boldsymbol{r}-\boldsymbol{r}'|}d\boldsymbol{r}' + v_{xc}(\boldsymbol{r})\right\}\phi_i(\boldsymbol{r}) = \varepsilon_i\phi_i(\boldsymbol{r}) \tag{2.2.1}$$

where $\phi_i(\boldsymbol{r})$ is the i-esim eigenfunction of the Hamiltonian, $v_{ext}(\boldsymbol{r})$ is the external potential (electronic interaction with fixed cores), ε_i is the Kohn-Sham eigenvalue associated to $\phi_i(\boldsymbol{r})$ eigenvector and $v_{xc}(\boldsymbol{r})$ is the exchange-correlation potential. The energy of the fundamental state has the form:

$$E_0[n(\boldsymbol{r})] = \sum_i \varepsilon_i + E_{xc}[n(\boldsymbol{r})] - \frac{1}{2}\int\int \frac{n(\boldsymbol{r})n(\boldsymbol{r}')}{|\boldsymbol{r}-\boldsymbol{r}'|}d\boldsymbol{r}'d\boldsymbol{r} - \int v_{xc}(\boldsymbol{r})n(\boldsymbol{r})d\boldsymbol{r}, \quad v_{xc}(\boldsymbol{r}) = \frac{\delta E_{xc}[n(\boldsymbol{r})]}{\delta n(\boldsymbol{r})} \tag{2.2.2}$$

where $E_{xc}[n(\boldsymbol{r})]$ is the exchange-correlation functional. From Eqs. 2.2.2 and 2.2.1, $E_0[n(\boldsymbol{r})]$ can be calculated once an explicit form of the exchange-correlation functional is provided. This functional contains all the information regarding the many-body correlation-exchange effects and is crucial to carry out accurate calculations.

The exchange-correlation functionals used in this work follow the generalized gradient approximation (GGA) to DFT. Within this approach, $E_{xc}[n(\boldsymbol{r})]$ has the general form:

$$E_{xc}^{GGA}[n(\boldsymbol{r})] = \int n(\boldsymbol{r})\varepsilon_{xc}\left[n(\boldsymbol{r}), \nabla n(\boldsymbol{r})\right]d\boldsymbol{r} \tag{2.2.3}$$

where ε_{xc} is the exchange-correlation energy per volume unit, which depends on the density and the gradient of the density for a given point $\boldsymbol{r}$. This makes the GGA-DFT a semi-local approximation in contrast with older local density approximations (LDA) where the exchange-correlation functional only depends on the density. The improvements that DFT-GGA introduces respect to DFT-LDA in adsoption energy and reaction barrier calculations make us able to construct accurate PES to run the molecule/surface dynamics, which is really sensible to the PES shape.

In this work, we have used three different DFT-GGA PES to run the 6D dynamics of $H_2(D_2)$/Cu(111) system. The first two, were obtained using the Perdew-Wang (PW91[81]) and the revised Perdew-Burke-Ernzerhof (RPBE[82]) exchange-correlation functionals. Both of them are widely applied in solid state calculations and yield to a semi-quantitative description of the reactive interaction of a molecule with a metal surface. More computational details are provided in Ref. [83]. The third one, was computed with an exchange-correlation functional defined within the specific reaction parameter (SRP) approach to DFT adapted to molecule/surface systems[78]. This DFT-SRP approximation yields to quantitative agreement with a wide set of observables for $H_2(D_2)$/Cu(111) system[79] and is briefly described in section 2.2.2.

2.2.2

Specific reaction parameter (SRP) approximation

The SRP approximation to DFT is a semiempirical method that has been recently proved to yield chemical description ($1\frac{kcal}{mol} \approx 43\,meV$) of several experiments for $H_2(D_2)$/Cu(111) system[79]. The main idea of this approximation is the definition of a new exchange-correlation functional (E_{XC}^{SRP}) mixing two other DFT-GGA functionals so that a mixing parameter (x) is fitted to reproduce a key experiment. By construction, one of this mixing functionals overestimates the values measured in the key experiment and the other one underestimates them. In this work, we have used the SRP exchange-correlation functional as defined in Ref. 79 within the BOSS approximation:

$$E_{XC}^{SRP} = xE_{XC}^{RPBE} + (1-x)E_{XC}^{PW91}, \qquad x = 0.43 \tag{2.2.4}$$

where the E_{XC}^{RPBE} and E_{XC}^{PW91} terms are the exchange-correlation parts corresponding to the RPBE and PW91 functionals. In our particular case, the (x) parameter was fitted to reproduce the experimental reaction probabilities from dissociative adsorption of D_2 on Cu(111)[84].

The fact that the calculations made with the SRP functional are more accurate than the PW91 and RPBE ones for a wide variety of experiments and conditions cannot be derived only from the fitting procedure. It has to be related with a better description of the reaction barrier heights, which are crucial to describe the dynamics of H_2(D_2) scattering from a Cu(111) surface. This is because the dynamics is very sensible to the reaction barrier heights that the impinging molecules encounter in their path, specially for those incidence energies that are lower than the calculated barriers. For instance, we can find or lose dynamical effects depending on the exchange-correlation functional we are using for the same problem (see sections 3.3 and 3.4).

2.2.3

Surface periodicity and supercell model

Crystals are periodic arrangements of atoms or molecules. They can be represented by a 3D Bravais Lattice ($\boldsymbol{R}$), which is an infinite set of points generated by all the integer linear combinations of three non-coplanar vectors called primitive vectors ($\boldsymbol{u}_1$, $\boldsymbol{u}_2$, $\boldsymbol{u}_3$):

$$\boldsymbol{R} = \left\{ \boldsymbol{r} = \sum_{i=1}^{3} \nu_i \boldsymbol{u}_i \,|\, v_i \in \mathcal{Z},\, \boldsymbol{u}_i \in \Re^3 \right\} \tag{2.2.5}$$

These vectors are three linear independent translations that define the smallest parallelepiped in $\boldsymbol{R}$ that can generate the periodic crystal structure only applying translation operations, which is known as the primitive cell. The set formed by the three primitive vectors $\{\boldsymbol{u}_i\}_{i=1}^{3}$ is a natural basis set for $\boldsymbol{R}$, although in crystallography, it is usually preferred to use bigger unit cells to make clear the crystal symmetry. In order to name a point of the lattice, a set of integer coefficients (ν_1, ν_2, ν_3) is used[85] (Eq. 2.2.5). In 3D space, there are 14 non equivalent spatial Bravais Lattices [1] classified in 7 lattice systems. Copper atoms are packaged in the face centered variety of the cubic system (fcc). In order to name a specific surface within a crystal system, we use the Miller indexes (h, k, l). These indexes can be defined as the coordinates of the smallest reciprocal vector that is normal to the surface plain. It is also equivalent to define these indexes (h, k, l) as inversely proportional to the intersection of the surface plain with the X, Y and Z axes respectively. In Fig. 2.2.1 we have plotted the fcc bulk structure of Cu and the Cu(111) and Cu(100) surfaces, which are the ones of interest for this work. Our theoretical study is focused on H_2(D_2) scattering from a Cu(111) surface but at some points our results are compared to experimental data provided for the Cu(100) surface (see chapter 3). In Fig. 2.2.2 we can see a detailed view of both surfaces, but we will only focus on the Cu(111) one (left

---

[1] 5 in the case of 2D space.

panel).

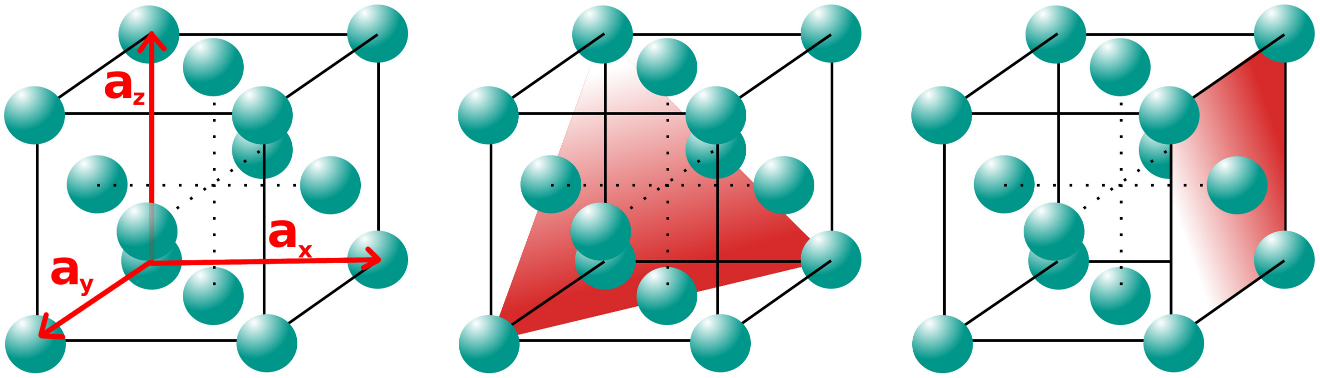

Figure 2.2.1: Left panel: Cu atoms arranged in a fcc structure. $\mathbf{a}_x$, $\mathbf{a}_y$, $\mathbf{a}_z$ basis vectors within cubic system. Center panel: Cu(111) surface. Right panel: Cu(100) surface.

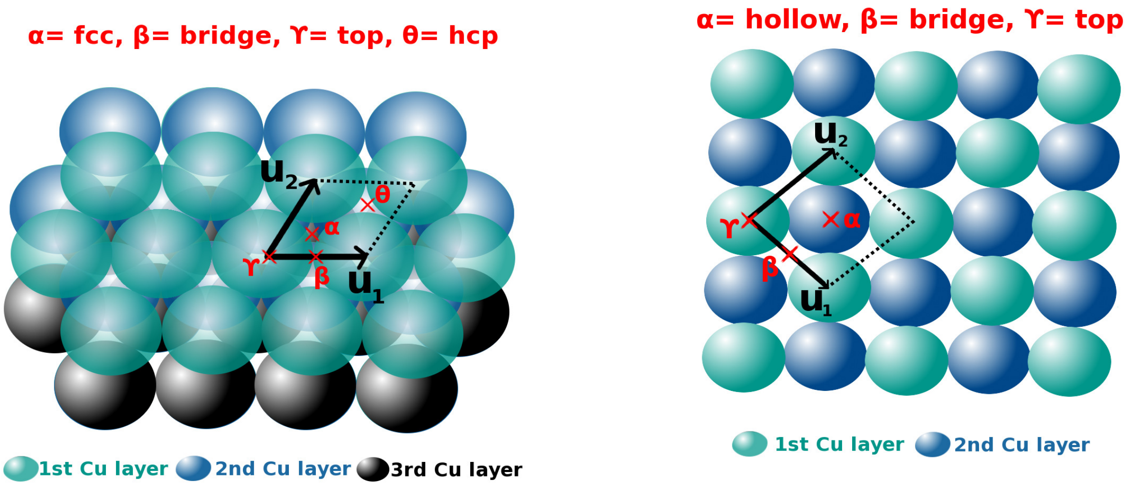

Figure 2.2.2: Left panel: top view of the first three Cu(111) surface layers. Right panel: top view of the first two Cu(100) surface layers.$\boldsymbol{u}_1$ and $\boldsymbol{u}_2$ are the primitive vectors of each surface. Greek red letters mark the high symmetry positions on the surface.

Within the DFT formalism (see section 2.2.1), the PES can be calculated solving the set of monoelectronic equations 2.2.1, where each equation only depends on 3 DOFs. However, as discussed above, for a molecule-surface system there are, in principle, an infinite number of electrons if further approximations are not taken. To face this problem, we can consider the surface as a 3D periodic structure so that Bloch theorem can be applied. The electronic wavefunction for a fixed crystal momentum $\boldsymbol{k}$ can be expanded over an infinite set of planewaves multiplied by an envelope function. Introducing this boundary to the Kohn-Sham ansatz give raise to a new set of equations in the reciprocal space:

$$\begin{cases} (1) \quad \phi_{n,\boldsymbol{k}}(\widetilde{\boldsymbol{Q}}_m, \boldsymbol{r}) = e^{i\boldsymbol{kr}} \sum_{\boldsymbol{G}} c_{n,\boldsymbol{k}+\boldsymbol{G}} e^{i\boldsymbol{Gr}} \\ (2) \quad \sum_{\boldsymbol{G}'} \left[\frac{\hbar^2}{2m}|\boldsymbol{k}+\boldsymbol{G}|^2\delta_{\boldsymbol{G}\boldsymbol{G}'} + v_{ext}(\boldsymbol{G}-\boldsymbol{G}') + v_H(\boldsymbol{G}-\boldsymbol{G}') + v_{xc}(\boldsymbol{G}-\boldsymbol{G}')\right] c_{n,\boldsymbol{k}+\boldsymbol{G}'} = \varepsilon_{n,\boldsymbol{k}} c_{n,\boldsymbol{k}+\boldsymbol{G}} \end{cases} \tag{2.2.6}$$

where $\boldsymbol{G}$ and $\boldsymbol{G}'$ are reciprocal lattice vectors, $c_{n,\boldsymbol{k}-\boldsymbol{G}}$ are the expansion coefficients over the plain waves basis set, $\varepsilon_{n,\boldsymbol{k}}$ is the energy for the $\phi_{n,\boldsymbol{k}}(\widetilde{\boldsymbol{Q}}_m, \boldsymbol{r})$ eigenvector, v_{ext}, v_H and v_{xc} are the Fourier transforms of the external, the Hartree and the exchange-correlation potentials respectively. Now, the problem with the infinite number of electronic DOF is substituted by the need of solving Eq. 2.2.6 for an infinite number of $\boldsymbol{k}$ momenta. However, as electronic wave functions evaluated near a certain value of $\boldsymbol{k}$ are quite similar, we only need to solve the electronic equation for a finite number of $\boldsymbol{k}$ vectors in the Brillouin zone to converge the total energy of the fundamental state for a given configuration $\widetilde{\boldsymbol{Q}}_m$[2]. We have to remark also that, in principle, the expansion in the plain waves basis set $\sum_{\boldsymbol{G}}^{\boldsymbol{G}_{cut}} c_{n,k-\boldsymbol{G}} e^{-i\boldsymbol{G}\boldsymbol{r}}$ is infinite, but in the simulations, it is truncated for an specific value of energy ($E_{cut} = \frac{\hbar^2}{2m}\boldsymbol{G}_{cut}^2$) so that plain waves with an associated kinetic energy higher than the cut off $|\boldsymbol{k} - \boldsymbol{G}| > \boldsymbol{G}_{cut}$ are neglected.

From the simulations point of view, solvig Eq. 2.2.6 using periodic boundary conditions for a molecule-surface system is not a straight forward task, because the system is only periodic in 2 dimensions (surface plane) . The most usual strategy followed to solve this problem is to create a suitable 3D supercell that can be repeated periodically in 3D-space while minimizing artifacts produced by the periodical assumption. First of all, a 2D unit cell (X, Y plane parallel to the surface) must be chosen so that the entire surface can be reproduced applying only translation operations. The chosen unit cell should be big enough to make negligible the spurious interaction between the periodic image of hydrogen molecules. Regarding the direction perpendicular to the surface (Z), the number of surface layers to be modeled should be large enough to reproduce bulk effects, and the vacuum space between adjacent surfaces should be wide enough to prevent hydrogen molecule interacting with the upper surface periodic image. For each electronic calculation, the hydrogen molecule have to be setted with the desired $\widetilde{\boldsymbol{Q}}_m$ conformation. The main advantage of this model is that we can use standard periodic calculations codes without any special modifications to obtain the electronic data we need to construct the PES. In Fig. 2.2.3, we have plotted a typical supercell model scheme.

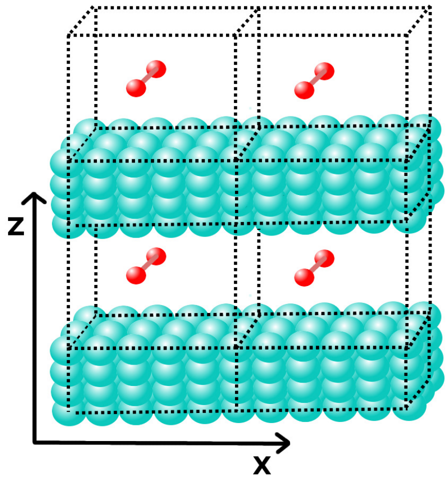

Figure 2.2.3: Supercell model expanded only in X and Z direction.

The PESs used in this work was obtained solving the DFT electronic equations with the DACAPO[86] code, which uses plane waves basis set to represent electronic wave functions and non local ultrasoft pseudopotentials (USSP) to simulate the ion cores.

---

[2] $\widetilde{\boldsymbol{Q}}_m$ refers to an specific value of the six spatial DOFs $(X, Y, Z, r, \theta, \phi)$ of the hydrogen molecule.

2.2.4

Corrugation reducing procedure (CRP)

In order to obtain a suitable complete PES to run the dynamics of a molecule/surface system it is necessary to solve Eq. 2.2.6 for all possible molecular configurations $\widetilde{\boldsymbol{Q}}_m$. Although DFT *ab initio* calculations and Bloch theorem make the system tractable, the computational cost to sample so many configurations is prohibitive. What it is done, instead, is to sample only a set of representative $\widetilde{\boldsymbol{Q}}_m$ and later on to apply an interpolation method to obtain the complete PES. In this case, the corrugation reducing procedure (CRP) interpolation method developed by Busnengo *et al.*[87] for diatomic molecules interacting with periodic surfaces was used.

The main problem that interpolation methods have to face is relative to the fact that the PES is not a smooth function so that a dense set of ab initio data is needed for an accurate interpolation. The main source of this roughness is the strong repulsive interactions between the molecule atoms and the surface atoms. To avoid this problem, the CRP method do not interpolate directly the PES (V^{6D}), but a smooth function ($\mathcal{I}^{6D}$) which is the result of subtracting to the 6D-PES the interaction of the individual atoms of the molecule with the surface ($\mathcal{R}_i^{3D}$, $i = A, B$):

$$\mathcal{I}^{6D}(X, Y, Z, r, \theta, \phi) = V^{6D}(X, Y, Z, r, \theta, \phi) - \mathcal{R}_a^{3D}(X_a, Y_a, Z_a) - \mathcal{R}_b^{3D}(X_b, Y_b, Z_b)$$

The interpolation of the smooth function $\mathcal{I}^{6D}$ is done with a cubic spline interpolation over (r, Z), Fourier series over (X,Y) and trigonometric functions for (θ, ϕ). In the last case, the molecular center of mass is kept fixed. The $\mathcal{R}_i^{3D}(X_i, Y_i, Z_i)$ (i=a,b) functions have to be chosen so that $V^{6D}(X, Y, Z, r, \theta, \phi)$ and $\mathcal{I}^{6D}(X, Y, Z, r, \theta, \phi)$ have the same symmetry.

In order to determine the $\mathcal{I}^{6D}$ function, $\mathcal{R}_a^{3D}$ and $\mathcal{R}_b^{3D}$ have to be known. These 3D-functions are not smooth due to the repulsive interaction between the atoms from the molecule and the atoms from the surface at short distances. Therefore, a similar interpolation procedure as done before can be applied to them:

$$\mathcal{J}_{n,i}^{3D}(X_i, Y_i, Z_i) = \mathcal{R}_i^{3D}(X_i, Y_i, Z_i) - \sum_{k=1}^{n} \mathcal{Q}_i^{1D}(R_k), \quad i = a, b$$

where $\mathcal{J}_{n,i}^{3D}$ is a smooth interpolation function and $\mathcal{Q}_i^{1D}(R_k)$ is the interaction of the i-esim adsorbing atom of the molecule and the k-esim nearest atom of the surface. $\mathcal{Q}_i^{1D}(R_k)$ has to be chosen so that the corrugation in $\mathcal{R}_i^{3D}(X_i, Y_i, Z_i)$ is reduced.

In order to simplify the calculations, the original Cu(111) surface symmetry (C_{3v}, see Fig. 2.2.2) was increased to C_{6v}. In Fig. 2.2.4 we have presented an schematic view of this conversion with some work variables. The only difference between the original surface and the new one with expanded symmetry is that the *fcc* and *hcp* positions are now considered equivalent by symmetry (they are almost degenerate in energy). This yields to a smaller irreducible Wiegner-Seitz cell, which means that we have to simulate the physics of the scattering problem over a smaller area, with the consequent decrease of computational cost.

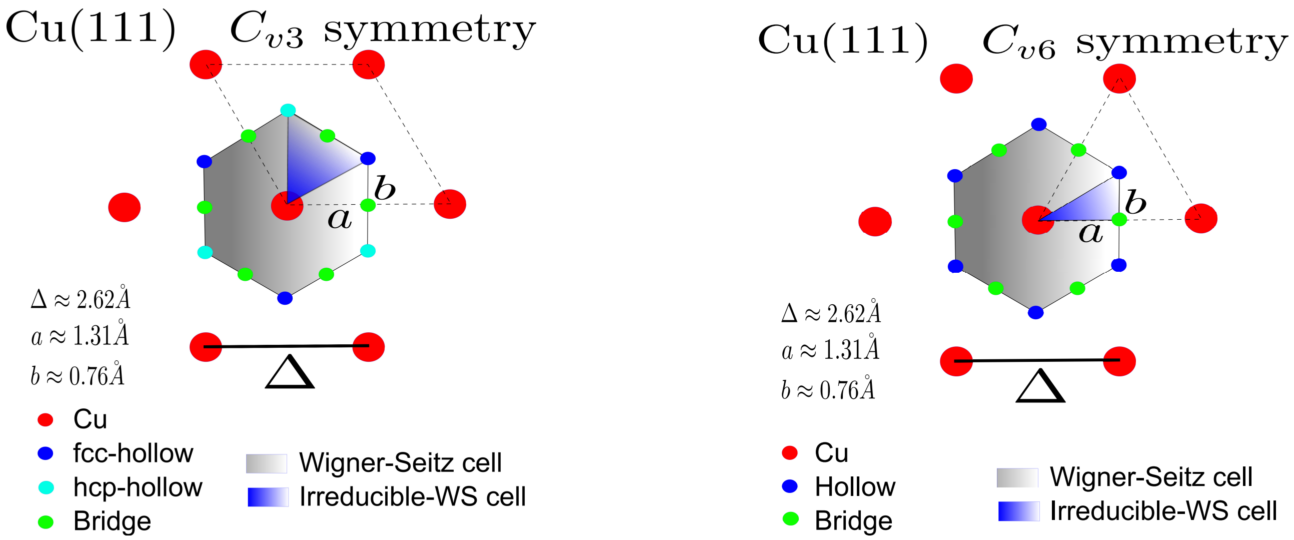

Figure 2.2.4: Irreducible Wigner-Seitz cell (shaded in blue) for the Cu(111) surface with C_{3v} (left graphic) and C_{6v} (right graphic) symmetry.

SECTION: 2.3

Adiabatic dynamics

Applying the Born-Oppenheimer approximation (BOA) to Eq. 2.1.2 allows us to separate the electronic and nuclear dynamics. This is also called the adiabatic approximation because the electrons adapt instantaneously to nuclei movement (see section 2.1). In this section we will discuss the theoretical methods used in this work to treat the quasi-classical (QC) and quantum (Q) dynamics of $H_2(D_2)/Cu(111)$ within the BOSS approximation.

2.3.1

Adiabatic quasi-classical (QC) dynamics

2.3.1.1 Equations of motion

Classically, the dynamics of a molecule/surface system can be obtained by integration of either the Newton equations of motion

$$M_i \ddot{\boldsymbol{R}}_i = -\boldsymbol{\nabla}_{\boldsymbol{R}_i} V(\{\boldsymbol{R}_j\}) \tag{2.3.1}$$

where $\boldsymbol{R}_i$ are the Cartesian spatial coordinates of the i-esim atom of the system, or the Hamilton equations of motion

$$\dot{\boldsymbol{q}}_k = \frac{\partial H}{\partial \boldsymbol{p}_k}, \quad \dot{\boldsymbol{p}}_k = -\frac{\partial H}{\partial \boldsymbol{q}_k} \tag{2.3.2}$$

where $\boldsymbol{q}_k$ and $\boldsymbol{p}_k$ are the generalized spatial coordinates and conjugate momenta of the system. Within the BOSS approximation the DOFs of the system are reduced to the molecular ones $(X, Y, Z, r, \theta, \phi)$ (see section 2.1) so that the Hamiltonian can be written:

$$H = \frac{1}{2m}(p_x^2 + p_y{}^{\mathbf{2}} + p_z^2) + \frac{1}{2\mu}\left(p_r^2 + \frac{p_\theta}{r^2} + \frac{p_\phi}{r^2 sen^2\theta}\right) + V^{6D}(X, Y, Z, r, \theta, \phi) \tag{2.3.3}$$

where V^{6D} is the 6D-potential energy surface, m is the total molecular mass and μ is the reduced molecular mass. In this work we have integrated the Hamilton equations of motion using the Bulirsch–Stoer algorithm[88]. During the integration process, we have imposed that the energy of each trajectory cannot fluctuate more than 0.1 meV at each integration step in order to maintain the energy conservation law.

For a given set of initial conditions, integrating Eq. 2.3.2 using the Hamiltonian written in 2.3.3 yields to a defined trajectory that describes the motion of an impinging $H_2(D_2)$ molecule. This trajectory is classified according to the different final channels that are typical from a molecule/surface system:

- **Reflection:** When the molecule reaches the initial Z_0 value (5.5 Å) with its velocity vector pointing to the vacuum.

- **Dissociative adsorption:** When the interatomic distance of the molecule is greater or equal to 2.22 Å, its radial velocity is positive $\left(\frac{dr}{dt} > 0\right)$ and the energy of each atom is negative.

- **One atom adsorption:** Same as the previous case, but only one atom has negative energy.

- **One atom absorption:** When the Z component of one of the atoms of the molecule is lower than the minimum Z value where the PES is known (0.05 Å) and its velocity vector is pointing to the surface.

- **Two atoms absorption:** When both atoms of the molecule reach previous conditions.

- **Dynamical trapping:** When the trajectory do not fulfill any of previous conditions before the integration time (15 ps) has finished, it is considered to be trapped on the surface.

2.3.1.2 Initial conditions

Within the QC trajectories method, the probability of each final channel for a given incidence energy and rovibrational quantum state is an average over the total number of trajectories computed. In order to obtain reliable results, the initial conditions for the $H_2(D_2)$ molecules have to be chosen uniformly from the set of possible conformations $\Omega_{E_t E_{int}} = \Omega_{E_t} \otimes \Omega_{E_{int}}$ in the phase space compatible with the translational energy E_t (incidence energy) and the internal energy E_{int} (determined by the rovibrational quantum state). This yields, in general, to two separate microcanonical ensemble distributions: one for translational degrees of freedom $\Omega_{E_t} = \{(p_X, p_y, p_z)\}$ depending on E_t, and one for internal degrees of freedom $\Omega_{E_{int}} = \{(r, \theta, \phi, p_r, p_\theta, p_\phi)\}$ depending on E_{int}. The (X, Y) DOFs are chosen randomly within the XY supercell plane.(Z) always has the same initial value (5.5 Å), which is big enough to consider the molecule/surface interaction negligible.

Regarding the distribution of $\Omega_{E_t} = \{(p_X, p_y, p_z)\}$, p_X and p_Y are setted to 0, because we are working under normal incidence conditions. Thus, we do not need any more a microcanonical ensemble to generate initial values for p_z. The only possible choice is: $p_z = -\sqrt{2mE_t}$. The negative sign makes sure that the velocity vector is pointing to the surface and not to the upper periodical image.

For the internal DOFs $\Omega_{E_{int}} = \{(r, \theta, \phi, p_r, p_\theta, p_\phi)\}$, we are able to sample (r, p_r) and $(\theta, \phi, p_\theta, p_\phi)$ independently[15] with a Montecarlo sampling method.

In this work, we have carried out calculations with 10^4 trajectories (N_{TOT}) to get statistical reliable results. The maximum absolute error (σ) in state resolved probability (p) at a given incidence energy is $5{\times}10^{-3}$, where σ is defined as $\sigma = \sqrt{\frac{p(1-p)}{N_{TOT}}}$.

2.3.1.3 Discretization of rotational and vibrational state

Variables used in classical dynamics are not quantified. Thus, in order to compare classical results with quantum calculations or state-resolved experiment we have to discretize these continuous variables.

In the case of the final rotational momentum (J_f), we have used the expression:

$$L^2 = J(J+1) \implies J_f = Int\left\{\frac{-1+\sqrt{1+4L^2}}{2}\right\} \qquad (a.u.) \tag{2.3.4}$$

where the operator $Int\{\,\}$ means that we just take the closest integer value to the real value inside the brackets. L^2 is the classical value of the angular momentum for the trajectory: $L^2 = \frac{p_\theta^2+p_\phi^2}{sen^2\theta}$. In the case of diatomic homonuclear molecules the discretization procedure has to take into account that only J_f values satisfying: $J_f = J_i \pm 2n$ with $n \in \mathbb{Z}$ and $J_f \geq 0$.

In the case of vibrational motion, we have followed the action variable formalism[89]:

$$S_r = \int_C p_r dr \implies v = Int\left\{\frac{S_r}{\pi} - \frac{1}{2}\right\}, \tag{2.3.5}$$

where the action variable (S_r) is integrated through the contour (c) between the classic turning points of (r) in the asymptotic potential $V(r)$ for the isolated molecule.

2.3.2

Adiabatic quantum dynamics: the wave packet method

The time evolution for a wave function representing our physical system ($X(\boldsymbol{Q},t)$) follows the time-dependent Schrödinger equation shown in Eq. 2.1.4. The solution for such equation can be written as:

$$X(\boldsymbol{Q},t) = \hat{U}(t)X(\boldsymbol{Q},0) = \left\{\hat{T}e^{-i\int_0^t \hat{H}dt'}\right\}X(\boldsymbol{Q},0) \tag{2.3.6}$$

where $\hat{U}(t)$ is the evolution operator and $\hat{T}$ is the time-ordering operator. If $\hat{H}$ does not depend on the time and $X(\boldsymbol{Q},0)$ is written as a supperposition of stationary wavefunctions for different energies $\psi(\boldsymbol{Q},E)$, we can simplified the expression 2.3.6 to:

$$X(\boldsymbol{Q},t) = e^{-i\hat{H}t}X(\boldsymbol{Q},0), \qquad X(\boldsymbol{Q},0) = \int_{-\infty}^{\infty}\psi(\boldsymbol{Q},E)dE \tag{2.3.7}$$

Therefore, the time-dependent wave function $X(\boldsymbol{Q},t)$ can be calculated making the time evolution of a supperposition of stationary $\psi(\boldsymbol{Q},E)$ wavefunctions for t=0.

The initial wavefunction $X_0(\boldsymbol{Q})$, is chosen so that the superposed $\psi(\boldsymbol{Q},E)$ wavefunctions are in the same rovibrational (v,j,m_j) quantum state and have the same parallel momentum ($\boldsymbol{K}_0$) to the surface:

$$X_0(\boldsymbol{Q}) = \int_{-\infty}^{\infty}\psi(\boldsymbol{Q},E)dE = \Phi_{vj}(r)Y_{jm_j}(\theta,\phi)\frac{1}{\sqrt{A}}e^{i\boldsymbol{K}_0\boldsymbol{R}_{xy}}G(z) \tag{2.3.8}$$

where $\Phi_{vj}(r)$ and $Y_{jm_j}(\theta,\phi)$ are the vibrational and rotational eigenfunctions for the isolated $H_2(D_2)$ molecule respectively, $\boldsymbol{R}_{xy}$ is the position vector projected on the parallele plane to the surface (X,Y), A is the surface unit cell area and G(z) is the wave-packet that describes the motion along the perpendicular direction to the surface (Z):

$$G(z) = \frac{1}{2\pi}\int_{-\infty}^{\infty} b(k_{z0})e^{ik_{z0}z}, \qquad b(k_{z0}) = \left(\frac{2\zeta^2}{\pi}\right)^{\frac{1}{4}} exp\left\{-(k_{av}-k_{z0})^2\zeta^2 + i(k_{av}-k_{z0})Z_0\right\} \tag{2.3.9}$$

where $b(k_{z0})$ is the Gaussian distribution for the momentum in Z, ζ is the width of the wave-packet in the momentum space and k_{av} is the average momentum.

In this work, we have used the split operatot method (SPO)[90;91] so that the time evolution operator in Eq. 2.3.7 can be approximated to:

$$e^{-i\hat{H}\Delta t} \approx e^{-i\hat{K}\frac{\Delta t}{2}} e^{-i\hat{V}\Delta t} e^{-i\hat{K}\frac{\Delta t}{2}} + O(\Delta t^3) \tag{2.3.10}$$

and the propagated wave-function can be written as:

$$X(\boldsymbol{Q}, t + \Delta t) = e^{-i\hat{K}\frac{\Delta t}{2}} e^{-i\hat{V}\Delta t} e^{-i\hat{K}\frac{\Delta t}{2}} X(\boldsymbol{Q}, t). \tag{2.3.11}$$

The error $O(\Delta t^3)$ rise from the fact that the kinetic and potential energy operators do not conmute. Eq. 2.3.11 have to be applied for short time intervals, otherwise the cumulative error can yield to unphysical results.

Once the initial wave-packet has evolved in time, the portion that is scattered back has to be analyzed at a given long enough value $Z = Z_\infty$ (distance to the surface) so that the interaction with the surface can be negligible. We have analyzed the asymptotic behavior of the wave-packet using the Balint-Kurti formalism[92] adapted for surface scattering[93]. Within this model, the scattered wavefunction is projected onto the free particle states $|n, m, v', j', m'_j >= |f >$:

$$C_f(Z_\infty, t) =< f|X(x, y, Z = Z_\infty, r, \theta, \phi, t) > \tag{2.3.12}$$

$$|f >= \phi_{v'j'}(r) Y_{j'm'_j}(\theta, \phi) \frac{1}{\sqrt{2\pi}} e^{ik_{zf}Z_\infty} \frac{1}{\sqrt{A}} e^{i(\boldsymbol{K}_0 + \boldsymbol{G}_{nm})\boldsymbol{R}_{xy}} \tag{2.3.13}$$

where Z_∞ is the distance to the surface at which we are analyzing the wavepacket, $\boldsymbol{G}_{nm}$ is a reciprocal surface vector associated with diffraction numbers (n, m) and v, j, m_j (v', j', m'_j) are the rovibrational quantum numbers for the initial (final) state. This procedure forms the basis of the so-called scattering amplitude formalism (SAF), where the S-matrix elements can be written as:

$$S_{i\to f} = \delta_{vv'}\delta_{jj'}\delta_{m_j m'_j}\delta_{0n}\delta_{0m} e^{-2ik_{z0}z_\infty} - \sqrt{\left(\frac{k_{z0}k_{zf}}{2\pi}\right)} \frac{A_f(z_\infty, E)}{Mb(-k_{z0})} e^{-ik_{zf}z_\infty} \tag{2.3.14}$$

$$A_f(z_\infty, E) = \int_0^\tau C_f(z_\infty, t) e^{iEt} dt \tag{2.3.15}$$

being $A_f(z_\infty, E)$ the Fourier transform of the coefficients $C_f(z_\infty, t)$, (τ) the propagation time and (i) the initial quantum state $|0, 0, v, j, m_j >$. The $S_{i\to f}$ matrix elements are crucial to calculate the scattering probabilities as a function of the incidence energy:

$$P_{i\to f}(E) = |S_{i\to f}|^2 \tag{2.3.16}$$

If we consider that the molecules can only be scattered or react on the surface, the reaction probability as a function of incident energy (E) and the initial quantum state (i) can be computed as:

$$R_i(E) = 1 - \sum_{\forall f} P_{i\to f}(E) \tag{2.3.17}$$

Once the wave-packet has been analyzed at $Z = Z_\infty$, it has to be subtracted from the environment, otherwise, it can give rise to unphysical interactions. The simplest way that we could think to resolve this problem, is just to remove the part of the wave packet that arrives to the analysis plane Z_∞. However, the introduction of such a hard discontinuity would lead to inaccuracies in the gradient calculation, which is needed to propagate the wave-packet. A suitable solution to this problem is to introduce an optical potential that slowly absorbs the wave-packet after it arrives to the analysis plane. A lot of different optic potentials have been studied in the literature[94]. The one used in the quantum mechanical calculations presented in section 3.3 can be written as:

$$V_{opt} = \begin{cases} -iA_2 \left(\frac{Z-Z_{min}}{Z_{max}-Z_{min}}\right)^2 & if \;\; Z_{min} \leq Z \leq Z_{max} \\ 0 & if \;\; Z < Z_{min} \end{cases} \tag{2.3.18}$$

where Z_{min} is chosen to be equal to Z_∞ and Z_{max} to the last grid point in Z direction. A_2 is a parameter that has to be chosen in order to absorb efficiently all the energies which are contained in the wavepacket.

An optical potential similar to the one in Eq. 2.3.18 is also used to remove the wave function in (r). Once the wavefunction reaches a value of (r) bigger than the dissociation limit (r_d), i.e. the molecule is assumed to be dissociated, it is not needed like in the previous case (it can yield to unphysical interactions).

SECTION: 2.4

Non-adiabatic dynamics: a friction-based method

The inclusion of non-adiabatic effects in full-quantum dynamics calculations can only be applied for systems with a few DOF at the present time. The high computational cost related to this kind of quantum formalism makes it prohibitive for molecule/surface simulations. However, great efforts have been made in the later years to develop "*cheaper*" friction-based methods that are easy to implement in classical molecular dynamics calculations. The non-adiabatic coupling between molecular DOF and electron-hole pair excitations can be introduced via dissipative friction forces that *de facto* substact energy from the classical equations of motion[95;96] . As this is not straight forward to proof, there are several approaches in the literature that yields to Langevind-like equations of motion using different approximations. In this work we have used the local density friction approximation[95;97] (LDFA).

2.4.1

Local density friction approximation (LDFA)

The LDFA describes the molecule/surface non-adiabatic interaction adding a dissipative force ($\boldsymbol{F}^{diss}$) to the classical equations of motion. This force is proportional to the velocity of the impinging particle times a scalar friction coefficient which depends on its position:

$$M_i \ddot{\boldsymbol{R}}_i = -\boldsymbol{\nabla}_{\boldsymbol{R}_i} V(\{\boldsymbol{R}_j\}) - \boldsymbol{F}_i^{diss} \tag{2.4.1}$$

where

$$\boldsymbol{F}_i^{diss}(\boldsymbol{R}_i, \dot{\boldsymbol{R}}_i) = \eta(\boldsymbol{R}_i)\dot{\boldsymbol{R}}_i \tag{2.4.2}$$

here, $\eta(\boldsymbol{R}_i)$ is the friction coefficient for the i-esim particle of the system at a given position $\boldsymbol{R}_i$ interacting with a homogeneous free electron gas (FEG) with density $n_o(\boldsymbol{R})$, which is equal to the ground state density of the isolated surface at $\boldsymbol{R}$. These coefficients are calculated individually for each atom of the molecule. This approximation is expected to introduce only small inaccuracies compared to correlated nuclei calculations in the case of homonuclear molecules[98].

The energy lost by a projectile traveling through the FEG may be modeled, in principle, within the time-dependent density functional theory (TDDFT) from the perturbed density induced by the impinging particle, but it was demonstrated[99] that for low incidence velocities we can obtain exactly the time-dependent result from a static DFT scheme. In addition, for vanishing velocities the dissipative force becomes proportional to the particle velocity so that it can be written like in Eq. 2.4.2. As a consequence, the dissipative force on the incident particle can be calculated in terms of the transport cross section $\sigma_{tr}(k_F)$ at the Fermi level[95], thus:

$$\boldsymbol{F}_i^{diss} = \dot{\boldsymbol{R}}_i n_0(\boldsymbol{R}_i) k_F \sigma_{tr}(k_F) \tag{2.4.3}$$

where

$$\sigma_{tr}(k_F) = \frac{4\pi}{k_F^2} \sum_{l=0}^{\infty} (l+1) sin^2 \left\{ \delta_l(k_F) - \delta_{l+1}(k_F) \right\} \tag{2.4.4}$$

$\delta_l(k_F)$ being the scattering phase-shifts at the Fermi level and k_F the Fermi momentum. From Eq. 2.4.2 and 2.4.3, we can write an explicit form of the friction coefficients:

$$\eta(\boldsymbol{R}_i) = n_0(\boldsymbol{R}_i) k_F \sigma_{tr}(k_F) \tag{2.4.5}$$

which is exactly valid for the low projectile velocity limit, i.e. for velocities lower than the Fermi velocity of the metal. This low velocity limit is enough to describe the physics of dissipative processes on thermal and hyperthermal atoms. LDFA is also able to take into account non-linear effects in the medium response and in the cross section calculation for the energy loss process. Thus, it can model the strong perturbation made by the slow impinging particle inside the FEG, which is necessary for a correct description of typical elementary gas-surface processes.

If the LDFA expression for the friction coefficients in Eq. 2.4.5 was directly implemented in the non-adiabatic QC dynamics calculations, we would need to compute the friction coefficients for each point in the 3D-space that the impinging atoms could reach. However, this procedure is not efficient because $\eta(\boldsymbol{R}_i)$ formally depends only on the electron density (n_0) given by the isolated surface. Thus, it is convenient to use an interpolation function that provides the friction coefficients as a function of the electronic density [100]:

$$\eta(r_s) = \sum_{i=1}^{n} A_i r_s^{B_i} e^{-C_i r_s} \tag{2.4.6}$$

being r_s the mean electronic radius of the FEG defined as $r_s = \left[\frac{3}{4\pi n_0}\right]^{\frac{1}{3}}$ and A_i, B_i and C_i three adjustable parameters for the i-esim term of the interpolation function. These parameters are fitted to $\eta(r_s)$ DFT *ab initio* calculations for a specific range of r_s. In the case of hydrogen atoms, it is only needed a one-term interpolation function to get an accurate fit to theoretical results (Fig. 2.4.1) where the fitting coefficients take the values $A_1 = 0.633$, $B_1 = 0.275$ and $C_1 = 0.558$.

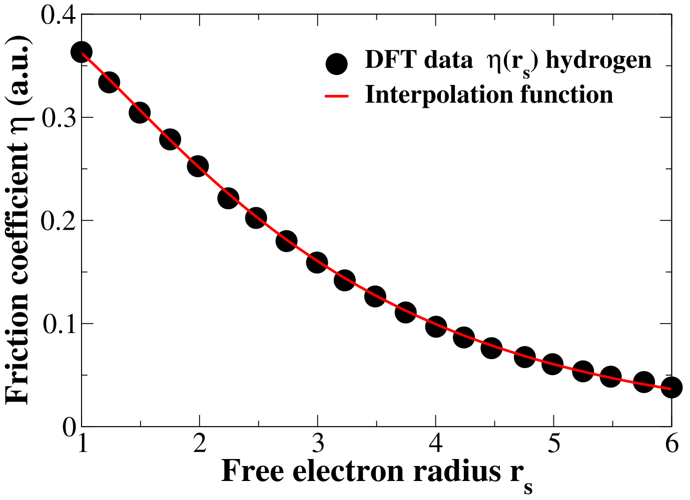

Figure 2.4.1: Friction coefficients for a hydrogen atom embedded in a free electron gas with density $\frac{1}{n_0} = \frac{4\pi}{3}r_s^3$. Black circles: DFT calculations within LDFA. Red line: one-term interpolation function fitted to theoretical data. Information extracted from Ref. [74]

CHAPTER 3

6-Dimensional dynamics results

SECTION: 3.1

Previous experimental results for $H_2(D_2)$/Cu(100)

Experiment of H_2 and D_2 state-to-state scattering from a Cu(100) surface (Fig 3.1.1) have been carried out by E. Watts *et al.*[40](H_2) and by L. C. Shackman *et al.*[41](D_2) aiming to measure the importance of vibrational and rotational inelastic processes. In these experiments, specific molecular rovibrational states (v, J) were selected via stimulated Raman pumping[101], and after scattered from a copper surface, under near-normal incidence conditions, survival and rotational excitation probabilities were measured as a function of the translational energies (E_i) using time-of-flight (TOF) measurements[39] and density-to-flux conversions. Due to experimental convenience, the chosen initial states were (v=1, J=1) for H_2 and (v=1, J=2) for D_2. Thus, our theoretical study has focused on these internal molecular states.

Despite the broad dispersion of experimental data, in Fig. 3.1.1 we can see a decrease of survival probabilities for both systems when translational energy increases. It is also clear that D_2/Cu(100) trends to have higher initial survival probabilities for every incident energy.

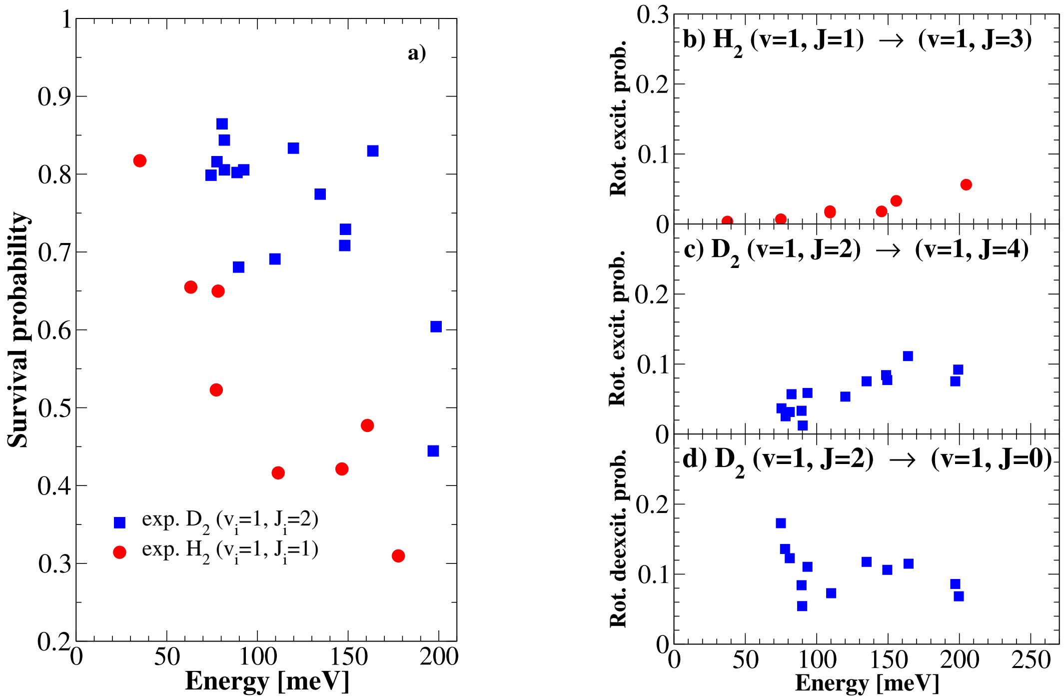

Figure 3.1.1: Left panel: vibrational survival probability as a function of the incidence energy; right panel: rotational excitation (**b**, **c**) and deexcitation (**d**) probabilities as a function of the incidence energy. Solid Blue squares: $D_2(v_i = 1,\ J_i = 2)$ experimental data from Ref. [41]. Solid red circles: $H_2(v_i = 1,\ J_i = 1)$/Cu(100) experimental data from Ref. [40]

SECTION: 3.2

Previous low-dimensional dynamics results

This isotope effect found experimentally (see section 3.1) has been considered as an evidence of a non adiabatic process. For example, Luntz *et al.*[80] have suggested that electron-hole (e-h) pair excitations could play a major role in $H_2(D_2)$+Cu inelastic scattering. Their conclusions were based on 3D quasi-classical non adiabatic calculations, where only two degrees of freedom (DOF) of the molecule, namely, the distance molecule-surface (z) and H-H bond length (r) and one DOF of the surface (modeling a thermal bath), are taken into account. Non adiabatic scattering probabilities were simulated with the friction tensor method[96] and with the forced oscillator model [102] (FOM). These low dimensional scattering results, which neglect rotational DOF, cannot be directly compared with the experimental probabilities but to experimental vibrational survival probabilities defined as $P_{sup}(v) = \sum_{J_f} P\left(v_f = v_i,\ J_f\right)$, which have been obtained by combining data from Fig. 3.1.1. Within this model, it has been also reported that adiabatic calculations could not reproduce the experiments[80]. In fact, in Ref. [80] was claimed that adiabatic calculations yield no vibrational deexcitation at all. The qualitative agreement between their theoretical non-adiabatic results and experiment is shown on Fig. 3.2.1.

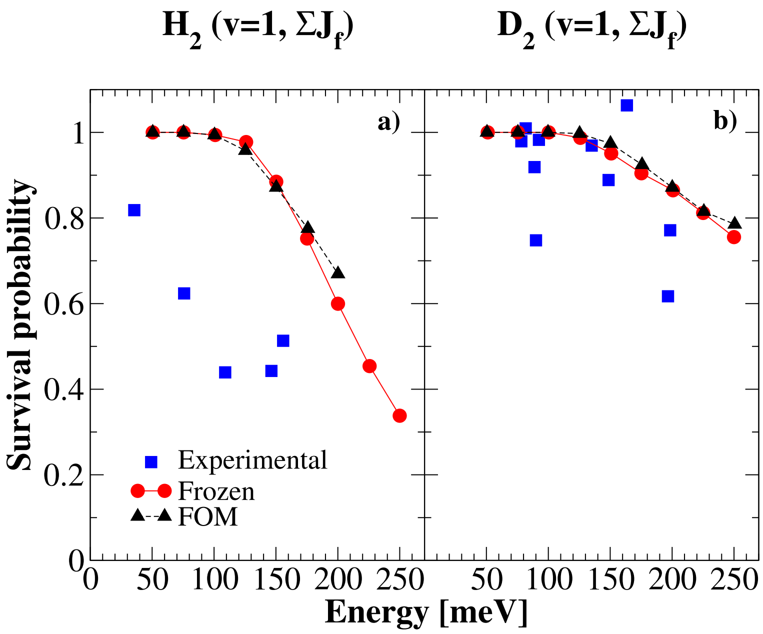

Figure 3.2.1: Vibrational survival probabilities (v_i = 1, J_i)⟶(v_f=1, ΣJ_f) for H_2/Cu(100) (**a**) and D_2/Cu(100) (**b**) as a function of incident energy. Solid blue squares: experimental data extracted from Refs. [40] (**a**) and [41] (**b**). Solid red line: 3D QC non adiabatic calculations with friction coefficients from Ref. [80]. Dashed black line: 3D QC non adiabatic calculations with FOM from Ref. [80]

SECTION: 3.3

Elastic and inelastic scattering analysis

From previous 3D study several questions rise: Is vibrational inelastic scattering of $H_2(D_2)$/Cu another example of failure of the Born-Oppenheimer static-surface (BOSS) approximation? Are low dimensional calculations suitable to study $H_2(D_2)$/Cu? In order to answer these questions we have performed 6D quasi-classical adiabatic and non adiabatic calculations. The methodology we have used is widely described in chapter 2. For the sake of theoretical convenience, we have used a Cu(111) surface instead of a Cu(100) one, but no major qualitative differences in the scattering are expected[40;80].

Our 6D adiabatic and non adiabatic quasi-classical (QC) SRP-PES rovibrational survival probabilities and rotational excitation and deexcitation probabilities are compared directly with experiment in Fig. 3.3.1. The reported experimental decrease of survival probability as a function of the incidence energy is quite well reproduced by both adiabatic and non adiabatic calculations (see Fig. 3.3.1, left panel). In fact, taking into account e-h pair excitations via a friction coefficients model hardly change adiabatic results. A closer look to this figure reveals that our model overestimates $H_2(v_i = 1,\ J_i = 1) \longrightarrow (v_f = 1, J_f = 1)$ elastic scattering, but it gives results that fit pretty well with D_2/Cu(100) measurements. However, quantitative agreement with experiment should not be expected due to several reasons. First, we are comparing theoretical results for Cu(111) with experimental data for Cu(100), therefore, some quantitative differences are envisaged. Second, the experiments were performed at a 500 k surface temperature and our method uses a frozen-surface scheme (static surface). Having these considerations in mind, the qualitative agreemet we have reached is really meaningful. On the other hand, there is no reason to argue that poor modelling of non adiabatic effects is to blame for the differences between theory and experiment rather than the exposed sources of error. In fact, our computed data are a clear evidence of the minor role played by e-h pair excitations in rovibrational elastic and inelastic scattering of $H_2(D_2)$/Cu(111). As already argued by Juaristi et al.[74], it is not the

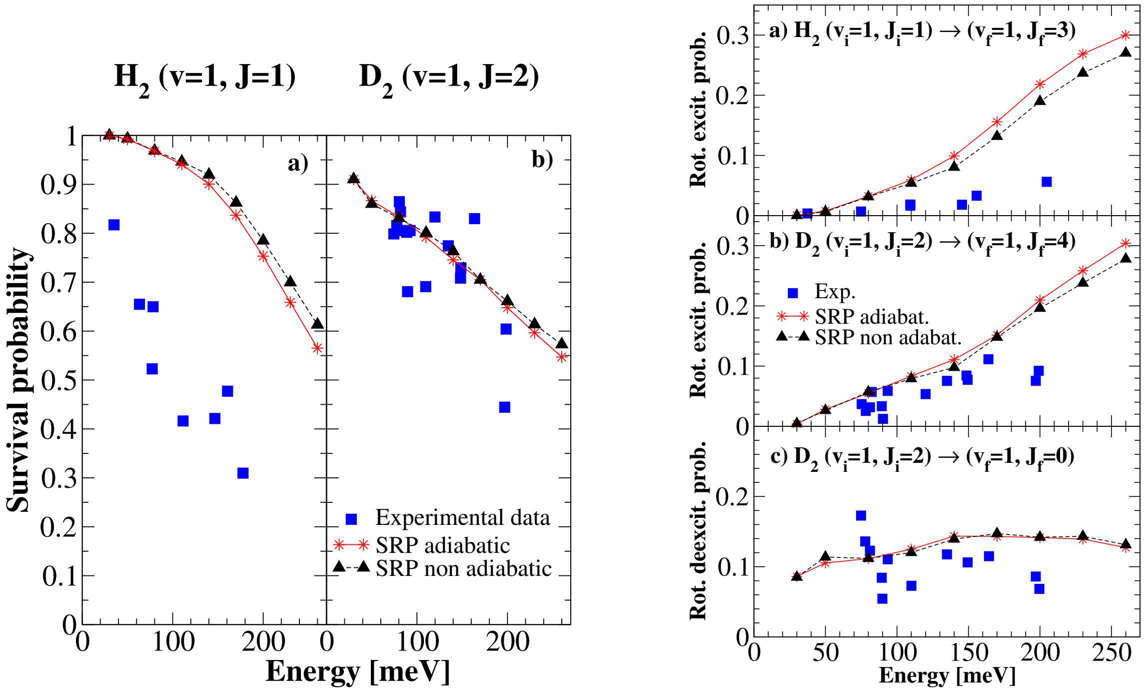

Figure 3.3.1: Left panel: (**a**) H_2/Cu(111) and (**b**) D_2/Cu(111) adiabatic and non adiabatic survival probabilities obtained with 6D quasi-classical calculations using SRP-PES compared with H_2/Cu(100)[40] and D_2/Cu(100) [41] experiments; right panel: theoretical and experimental rotational (de)excitation probabilities extracted from the same references. Red solid lines: SRP 6D QC adiabatic calculations. Black dashed line: SRP 6D QC non-adiabatic calculations. Blue solid squares: experimental data from Refs. [40;41].

friction tensor who extracts energy from the system but the dissipative force involved (see chapter 2) which is also proportional to the velocity of the particle. Thus, the slowing down of the molecule near the surface, i. e. near the high density zones, would explain the marginal corrections added by the friction coefficients model.

Similar qualitative results are obtained for the PW91-PES and the RPBE-PES (Fig. 3.3.2). In Fig. 3.3.2, we have plotted adiabatic and non-adiabatic survival (left panel) and rotational inelastic (right panel) probabilities for $H_2(v = 1, J = 1)$ and $D_2(v = 1, J = 2)$ in a similar way than in Fig. 3.3.1 but using PW91-PES and RPBE-PES QC calculations. Results computed with the SRP-PES have been also included for the shake of completeness. From Fig. 3.3.2, we can see that PW91-PES survival probabilities trend to be lower than those calculated using the RPBE-PES (left panel). Thus, the former PES favors inelastic scattering compared to the latter one. This tendency is much more evident as incidence energy increases. Differences between both functionals will be further analyzed it in section 3.4. Comparing $H_2(v = 1, J = 1)$ and $D_2(v = 1, J = 2)$ survival probabilities computed with different PES (Fig.3.3.2, left panel **a** and **b**), we can realize that calculations with PW91-PES clearly exhibit the isotopic effect shown in experiment[40;41] (lower survival probabilities for H_2) since in the case of RPBE-PES the effect practically disappears. This behavior can be justified by the too high reaction barriers present on the latter PES[78;83]. Regarding rotational inelastic scattering (Fig. 3.3.2 , right panel), we can see that PW91-PES probabilities are higher for excitation processes ($H_2(v_i = 1\, J_i = 1) \longrightarrow (v_f = 1, J_f = 3)$, $D_2(v_i = 1\, J_i = 2) \longrightarrow (v_f = 1, J_f = 4)$) and lower in the deexcitation case $D_2(v_i = 1\, J_i = 2) \longrightarrow (v_f = 1, J_f = 0)$. From results in figures 3.3.1 and 3.3.2 we can also rule out the influence of the functional on isotope effect observed for rovibrationally inelastic scattering for those functionals yielding reaction barriers comparable to experimentally estimated ones, i.e., for PW91 and SRP.

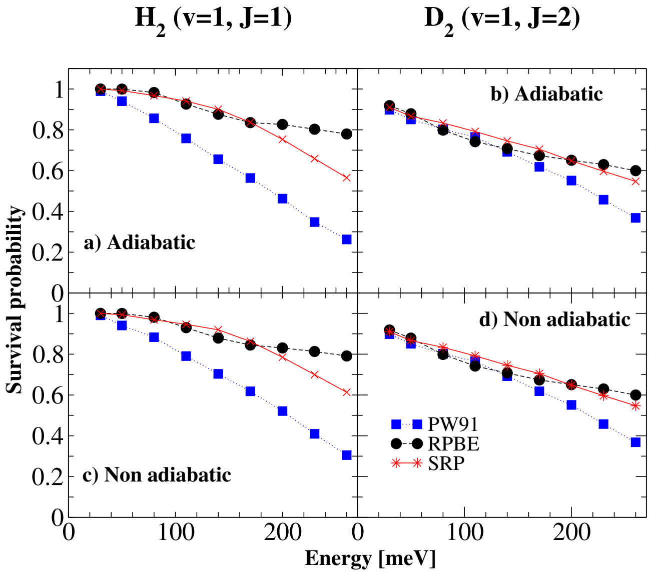

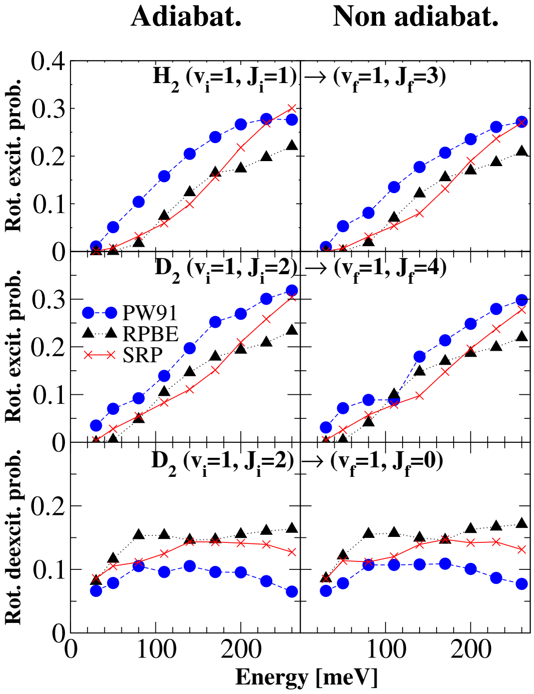

Figure 3.3.2: Left graphic: survival 6D QC adiabatic (**a**, **b**) and non adiabatic (**c**, **d**) probabilities for $H_2(v_i = 1, J_i = 1)$ (panels on the left) and $D_2(v_i = 1, J_i = 2)$ (panels on the right) as a function of incident energy. Right graphic: rotational excitation/deexcitation adiabatic (panels on the left) and non-adiabatic (panels on the right) probabilities as a function of the incidence energy. (**a**) $H_2(v_i = 1, J_i = 1) \longrightarrow (v_f = 1, J_f = 3)$; (**b**) $D_2(v_i = 1, J_i = 2) \longrightarrow (v_f = 0, J_f = 4)$; (**c**) $D_2(v_i = 1, J_i = 2) \longrightarrow (v_f = 1, J_f = 0)$. Blue dashed lines: PW91 6D QC calculations. Red solid lines: SRP 6D QC calculations. Black dotted line: RPBE 6D QC calculations.

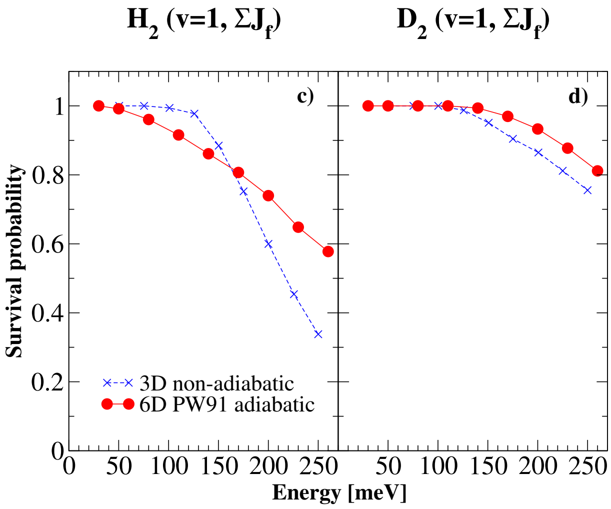

Figure 3.3.3: Transition probability $H_2(v_i = 1, J_i = 1) \longrightarrow (v_f = 1, \Sigma J_f)$ (left panel) and $D_2(v_i = 1, J_i = 2) \longrightarrow (v_f = 0, \Sigma J_f)$ (right panel) as a function of the incidence energy. Red solid line: 6D QC adiabatic calculations using the PW91-PES. Dashed blue line: 3D QC non-adiabatic calculations using a PW91-PES, from Ref. [80]

In order to compare our results with those of Luntz and Co.[80], we have summed our state-to-state vibrational deexcitation probabilities (PW91-PES) over all final rotational states (J_f) . In figure 3.3.3 we compare our 6D adiabatic results with the 3D non-adiabatic ones from Ref. [80] for $H_2(v = 1, J = 1)$ (Fig. 3.3.3**a**) and $D_2(v = 1, J = 2)$ (Fig. 3.3.3**b**). From this figure we can see that the shape of the adiabatic and non adiabatic curves are qualitatively similar. It seems that the low dimensional model including non adiabatic effects somehow compensates the lack of rotational DOF, giving qualitative good results in comparison with experiment. Therefore, our QC study points out the importance of carrying out multidimensional dynamics in order to avoid erroneous interpretations of the role played by non adiabatic effects in the dynamics of $H_2(D_2)$ scattered from copper.

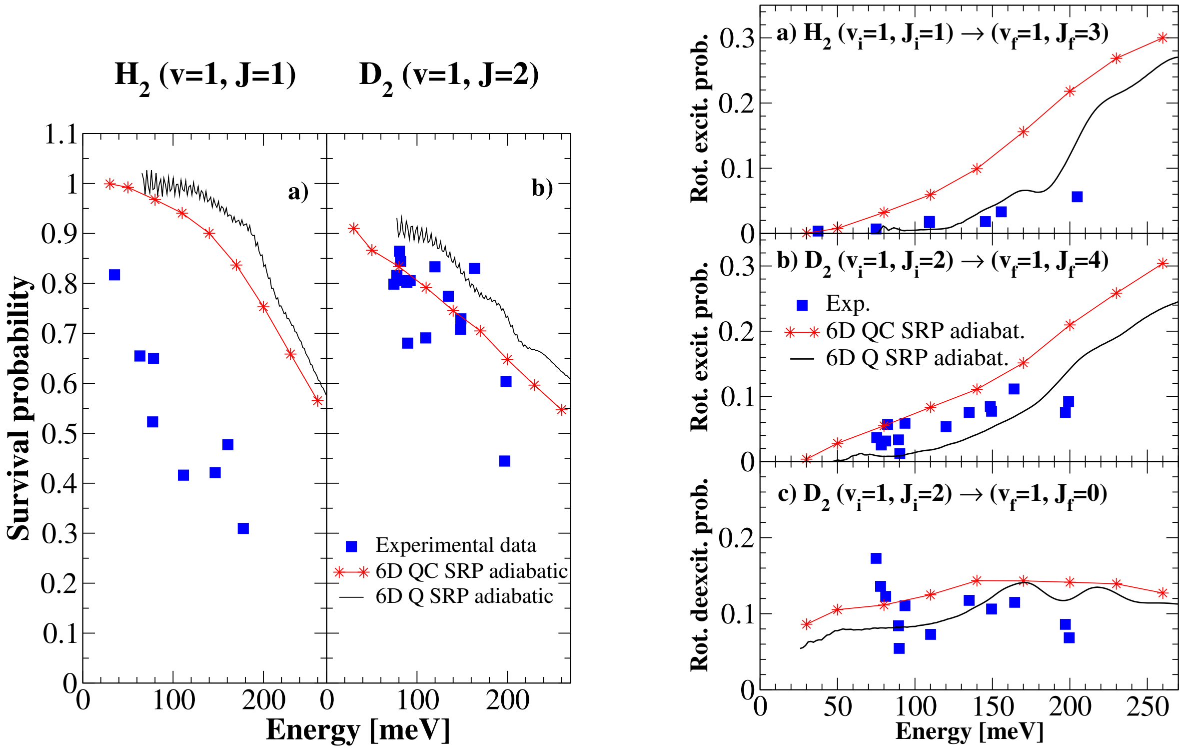

Figure 3.3.4: Left panel: vibrational survival probability as a function of the incidence energy for $H_2(v_i = 1, J_i = 1)$(**a**) and $D_2(v_i = 1, J_i = 2)$(**b**) Right panel: rotational excitation/deexcitation probability as a function of the incidence energy. (**a**) $H_2(v_i = 1, J_i = 1) \longrightarrow (v_f = 1, J_f = 3)$; (**b**) $D_2(v_i = 1, J_i = 2) \longrightarrow (v_f = 0, J_f = 4)$; (**c**) $D_2(v_i = 1, J_i = 2) \longrightarrow (v_f = 1, J_f = 0)$. Blue solid squares: experiments from Refs. [40;41]. Black solid line: SRP 6D Q adiabatic calculations. Dashed red line: SRP 6D QC adiabatic calculations.

To discard spurious effects in our previous calculations due to the use of classical dynamics, we have compared our results with quantum (Q) calculations. In Fig. 3.3.4 we have plotted Q and QC survival and inelastic rotational probabilities. Experimental values are also shown for the sake of completeness. From the left panel of Fig. 3.3.4 we can see that quantum results also reproduce the isotopic effect reported in experiment. From the right panel, rotational excitation and deexcitation QC probabilities are systematically higher than those from Q calculations. Quantitative discrepancies between Q and QC dynamics are due to one main source of error: the discretization method used in the latter (see chapter 2) which trends to overestimate inelastic processes. Nevertheless, as it is clear that both approaches can qualitatively explain the experiments done by E. Watts *et al.*[40] and by L. C. Shackman *et al.*[41], we conclude that our classical methodology is appropriate to study this system.

So far we have shown that non-adiabatic dynamics is not mandatory to mimic the $H_2(D_2)/Cu(111)$ scattering experimental results. No matter the PES (SRP or PW91) or the kind of dynamics (QC, Q) we use, the adiabatic approach always present the isotopic effect observed in experiment. Now, we are going to analyze deeply our computed 6D QC data in order to understand why vibrational survival probabilities for D_2 are higher than those for H_2. In Fig. 3.3.5 we show all our computed adiabatic and non adiabatic rovibrational probabilities, for the 3 PES (PW91, SRP, RPBE) considered in this work, defined as $H_2(v_i = 1, J_i = 1) \longrightarrow H_2(v_f, J_f)$, together with dissociative adsorption probabilities. In this figure, we can see the rotational inelastic channels measured in the experiments, i.e. $(v_i = 1, J_i = 1) \longrightarrow (v_f = 1, J_f = 3)$ for H_2, and $(v_i = 1, J_i = 2) \longrightarrow (v_f = 1, J_f = 4)$ and $(v_i = 1, J_i = 2) \longrightarrow (v_f = 1, J_f = 0)$ for D_2, in addition to other possible vibrational elastic and inelastic scattered channels. From Fig. 3.3.5 (**B** and **D** panels) we can see once again that non-adiabatic effects slightly introduce any change in the computed probabilities for any scattering channel. If we focus on the insets of Fig. 3.3.5, we realice that H_2 has more effective vibrational deexcitation channels than D_2. In Fig. 3.3.6 we have compared vibrational elastic and inelastic (deexcitation) probabilities (summed over all J_f) and reactive probabilities. This figure can help us to understand the isotope effect. At low incident energy, there is not vibrational deexcitation process taking place and vibrational survival profiles present the same behavior. However, when we reach higher energies (150 meV), vibrational deexcitation and dissociative adsorption channels of H_2/Cu(111) start to play a major role in the scattering process. In the case of D_2, even at the highest E_i, the reactive channel is completely absent and vibrational deexcitation probabilities are lower than those for H_2 by almost one order of magnitude. Hence, from figures 3.3.5 and 3.3.6 we conclude that the experimental isotope effect reported in Refs. [40;41] is a consequence of the higher vibrational deexcitation and dissociative adsorption probabilities exhibited by H_2 molecules. We have provided a more detailed analysis of this effect in section 3.4.

Eventually, it is worth to comment on experimental results for H_2 at low energy (≈50 meV). In Ref. [40], it was reported that the flux of incident molecules with the vibrational state $v_i = 1$ did not coincide with the flux of scattered molecules with the same vibrational state, i.e. it was reported that survival probabilities are smaller than 1. In Ref. [40] was speculated that the loss of flux was due to the existence of intense deexcitation process to the $(v_i = 1, J_i = 1) \longrightarrow (v_f = 0, J_f = 3)$ and $H_2(v_i = 1, J_i = 1) \longrightarrow H_2(v_f = 0, J_f = 1)$ inelastic channels. However, our calculations do not show important vibrational deexcitation at low incident energies. In fact, independently of the PES, the dynamics (Q, QC) or the approach (BOSS, non adiabatic) used, we always obtain that the sum over all rotational scattering states with $v_f = 1$ is 1 at these energies. Thus, it is still an open question why experimentally the $(v_i = 1, J_i = 1) \longrightarrow (v_f = 1, \Sigma J_f)$ probability is found to be less than 1. At this point, we should emphasize that although it has been suggested that survival and rotational excitation probabilities for $H_2(v_i = 1, J_i = 0)$/Cu(111) are almost independent with the change of surface temperature[103], quantitative agreement with the experiment will probably require the proper introduction of surface phonons in the theoretical model[104;105]. Finally, we should take into account the dispersion of the experimental data. Measurements at the same energies show data differing up to 20%. Therefore as a first approximation, this number could be taken as the experimental error bar.

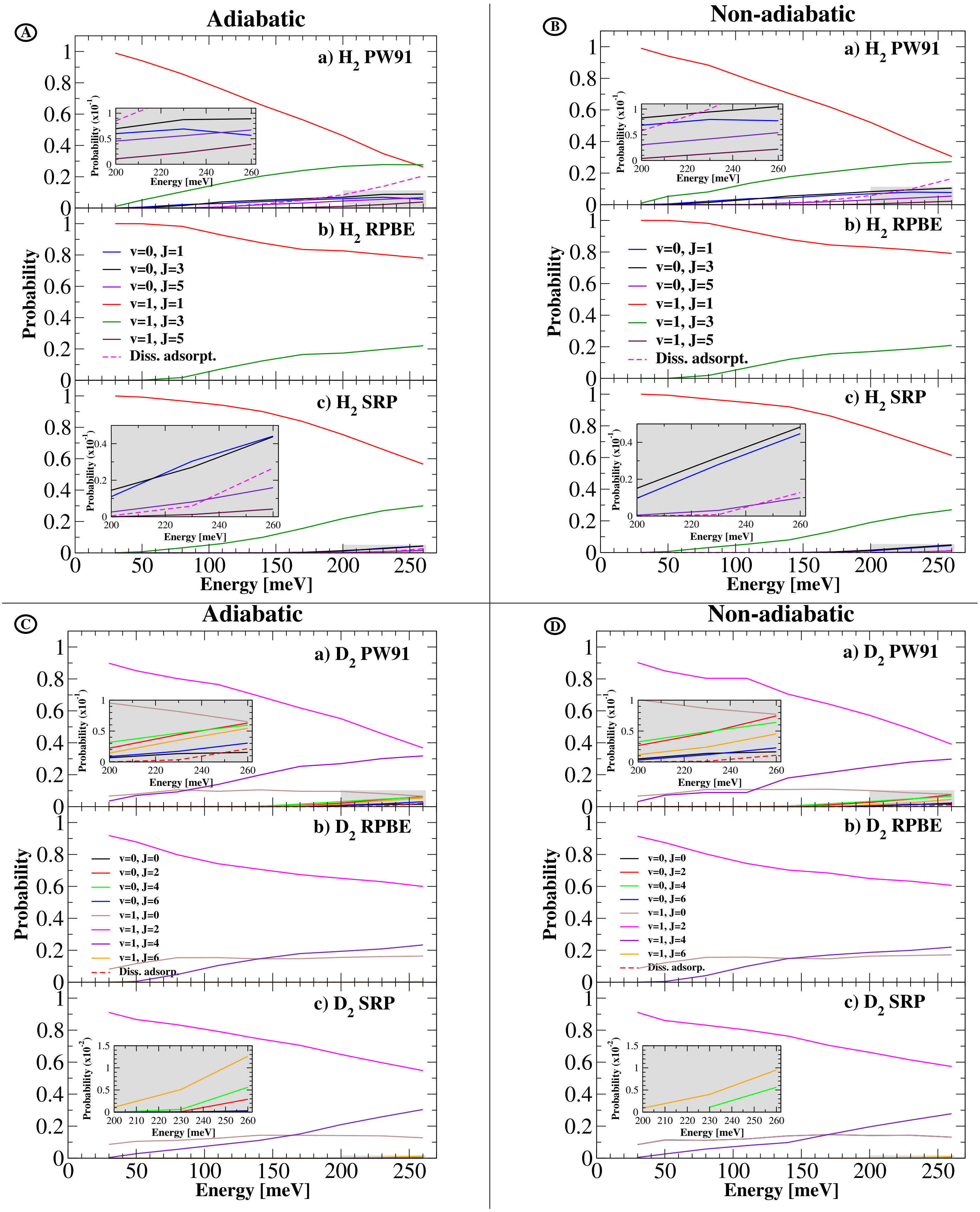

Figure 3.3.5: H_2(v=1, J=1)/Cu(111) (**A**, **B**) and D_2(v=1, J=2)/Cu(111) (**C**, **D**) rovibrational elastic and inelastic probabilities as a function of incidence energy. For each panel: (**a**) PW91-PES, (**b**) RPBE-PES and (**c**) SRP-PES used. Non adiabatic effects via friction coefficients included in **B** and **D** panels.

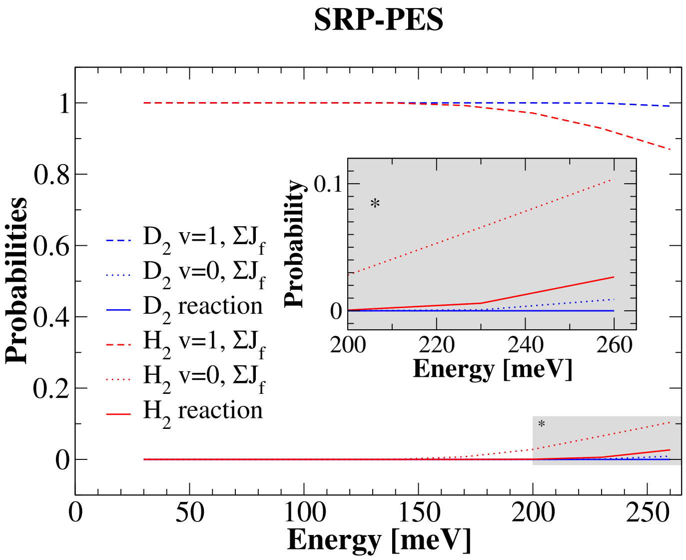

Figure 3.3.6: Dissociative adsorption probabilities (solid lines), vibrationally elastic survival probabilities ($v_i = 1,\ J_i) \longrightarrow (v_f = 1,\ \Sigma J_f)$ (dashed lines) and vibrationally inelastic probabilities $(v_i = 1,\ J_i) \longrightarrow (v_f = 0,\ \Sigma J_f)$ (dotted line) as a function of incidence energy for $H_2(v_i = 1,\ J_i = 1)/Cu(111)$ (red) and $D_2(v_i = 1\ J_i = 2)/Cu(111)$ (blue).

SECTION: 3.4

Classical turning points analysis

We have shown in section 3.3 that within the Born-Oppenheimer static-surface approximation (BOSS) we have been able to reproduce qualitatively the experimental isotope effect measured by E. Watts *et al.*[40] and by L. C. Shackman *et al.*[41] for $H_2(D_2)/Cu(100)$ scattering using a Cu(111) surface. We have also provided a key idea to understand this isotope effects found in experiment without the need of invoking any non-adiabatic effect; vibrational deexcitation $H_2(v_i = 1,\ J_i) \longrightarrow H_2(v_f = 0,\ \Sigma J_f)$ and dissociative adsorption channels for H_2 are more efficient than for D_2 (see Fig. 3.3.6). But, until now we have not provided any explanation for this phenomenon. In this section we are going to take advantage of a classical trajectory method in order to explain the underlying physical processes that are responsible for the isotope effect.

A classical trajectory does not allow the molecules to tunnel across the PES. The molecule is scattered when it encounters with a reaction barrier higher than its own translation energy. However, we have to take into account also the energy transfer from vibration to translation (V-T) due to the coupling with the surface, which allows the energy exchange between molecule DOF. This extra translational energy allows the molecule to overcome *more barriers*, and therefore, to get closer to the surface. *G. R. Darling* and *S. Holloway* have shown[10;25] that T-V energy transfer is enhanced in late barrier systems (systems which have reaction barriers close to the surface, as $H_2(D_2)/Cu$) due to the high curvature of the PES in front of the reaction barrier. Hence, if V-T energy transfer is favored, a higher number of molecules can reach high curvature zones close to the surface, and therefore, a higher proportion of vibrationally inelastic scattered molecules is expected. In Fig. 3.4.1 we have plotted the distribution of classical turning points for the SRP-PES as a function of the distance to the surface (Z) for $H_2(v_i = 1,\ J_i = 1)$ and $D_2(v_i = 1,\ J_i = 2)$ at two incident energies (80, 230 meV). From Fig. 3.4.1, it can be seen that H_2 molecules are able to get closer to the surface than D_2 molecules, specially at 230 meV. This observation seems to be reasonable, because H_2 vibrational energy levels are $\sqrt{2}$ times higher than those from D_2. Thus, the vibrational softening, i.e. the energy transfer from vibration to translation, is expected to be higher for H_2 than for D_2. Hence, we hypothesize that the higher vibrational deexcitation effectiveness found in $H_2/Cu(111)$ is due to the capability of H_2 molecules to explore deeper zones in the PES, which enhances the coupling to the reaction path curvature[10;25]. To further analyze classical trajectory results, let us focus on the classical turning point distribution at high energy (Figs. 3.4.1, **b** and **c**). These distributions present a double peaked structure, which reveals that a number of molecules can get rather close to the surface . If we compare panel (**b**) (H_2) and panel (**d**) (D_2) we clearly see that the intensity of the first peak (the closest to the surface) is significantly higher in the former case. Let us perform a detailed analysis of this phenomenon.

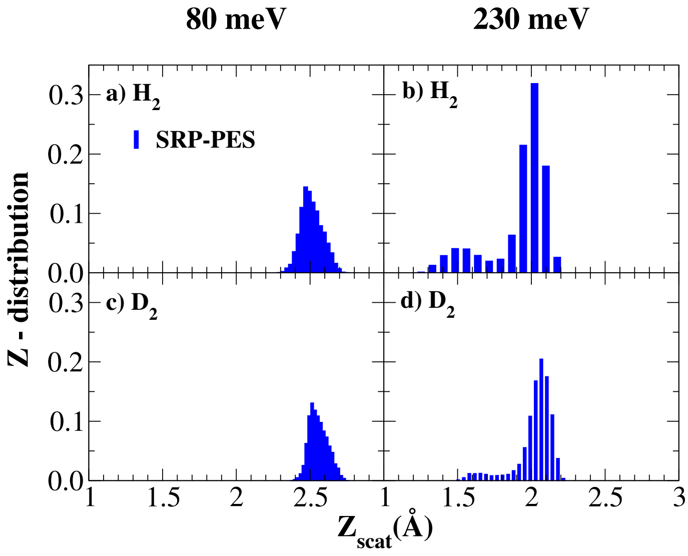

Figure 3.4.1: Distribution of classical turning points (Z_{scat}) of the molecules scattered from the SRP-PES as a function of molecule-surface distance.(**a**) $H_2(v = 1, J = 1)$, E_i=80 meV; (**b**) $H_2(v = 1, J = 1)$, E_i=230 meV; (**c**) $D_2(v = 1, J = 2)$, E_i=80 meV; (**d**) $D_2(v = 1, J = 2)$, E_i=230 meV.

In Fig. 3.4.2 we have projected the classical turning points XY-distribution over the irreducible Wigner-Seitz (IWS) cell of the Cu(111) surface (adapted from C_{3v} to C_{6v} symmetry, see chapter 2). In addition, we have projected separately those scattered trajectories that belong to the two different peaks (if present). Fig. 3.4.2 shows that the first peak (the closer to the surface) corresponds to those molecules which are reflected preferably over the top-site (panels **C-a** and **D-a**). Trajectories that cannot reach such close-to-surface zones (panels **C-b**, **D-b**) are scattered preferably on the bridge-site and corresponds to the second peak. At that point, we should point out that the top-site is not the one with the minimum reaction barrier, in fact, the minimum reaction barrier for H_2/Cu(111) system is located at the bridge-site[83] (see Fig. 3.4.3). Thus, molecules that reach closer zones to the copper surface do not follow the minimum reaction path. This phenomenon has also been reported by D. A. McCormack *et al.*[76] for dissociation of vibrationally excited H_2 molecules on Cu(100). Furthermore, in Ref. [30], it has been also shown for H_2/Cu(100), that top-site collisions are effective promoting vibrational inelastic scattering due to the high curvature in front of this barrier. The same reference suggests that a similar phenomenon should be seen for the Cu(111) surface. Our results corroborate that hypothesis. Therefore, from Fig. 3.4.2 and the support of Ref [30], we conclude that the higher vibrational deexcitation effectiveness found theoretically in H_2/Cu(111) is due to the higher number of incident H_2 molecules that are scattered over the top-site close to the surface compared to D_2 (see Fig.3.4.2 **B** and **D** panels), which favors rovibrational inelastic scattering. This effect only rises when the initial translational energy is enough to reach those zones of the PES where vibration (r) and translation (Z) are coupled (>150 meV, see Fig. 3.3.6) and V-T energy transfer is enhanced. Similar effects should take place for $H_2(D_2)$/Cu(100).

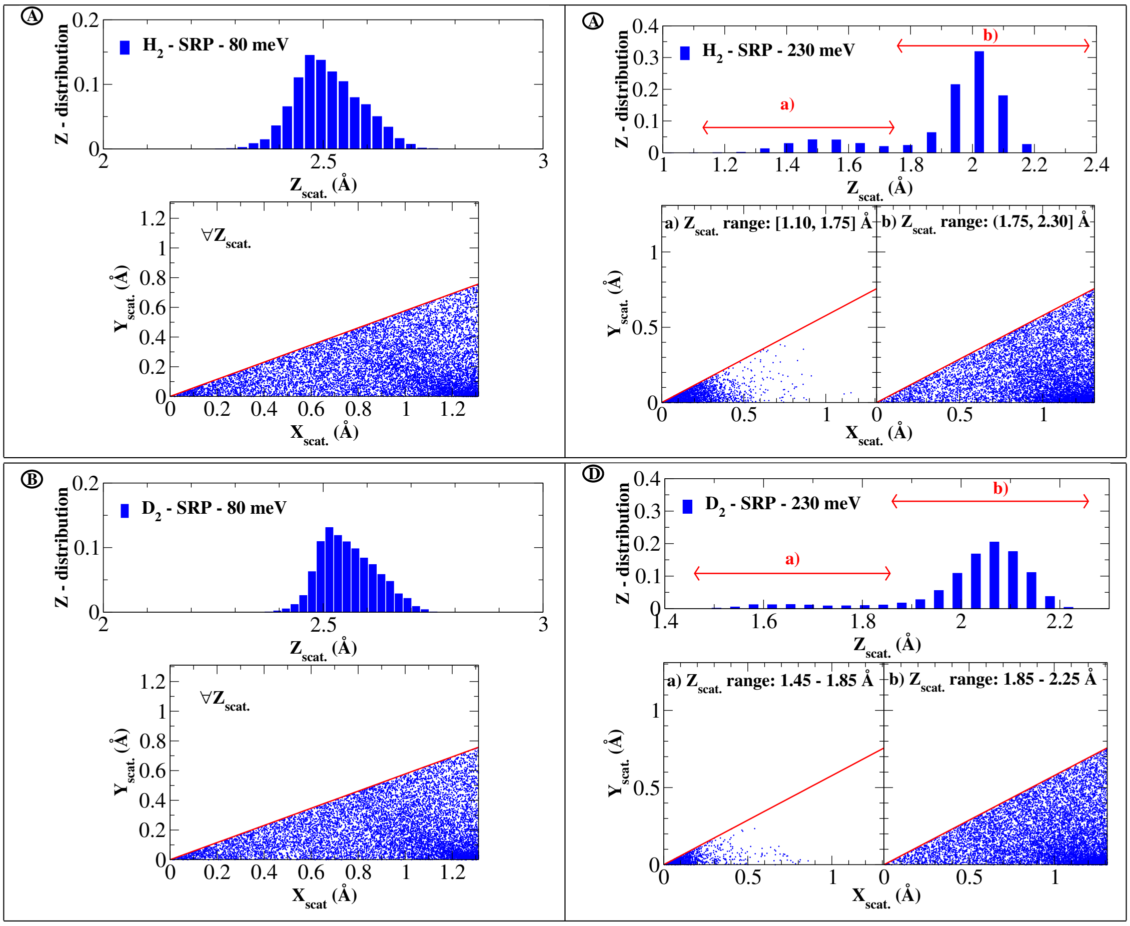

Figure 3.4.2: For each graphic (**A**, **B**, **C**, **D**): Top panel, distribution of the classical turning points (Z_{scat}) of H_2 molecules from the SRP-PES for 80 meV (**A**, **B**) and 230 meV (**C**, **D**); bottom panel, $X_{cm}Y_{cm}$-distribution of the classical turning points for the scattered molecules, projected on the IWS cell (red solid line), for the Z intervals marked in top panel. (**A**) $H_2(v_i = 1, J_i = 1)$, E_i=80 meV. (**B**) $H_2(v_i = 1, J_i = 1)$, E_i=230 meV. (**C**) $D_2(v_i = 1, J_i = 12)$, E_i=80 meV. (**D**) $D_2(v_i = 1, J_i = 2)$, E_i=230 meV.

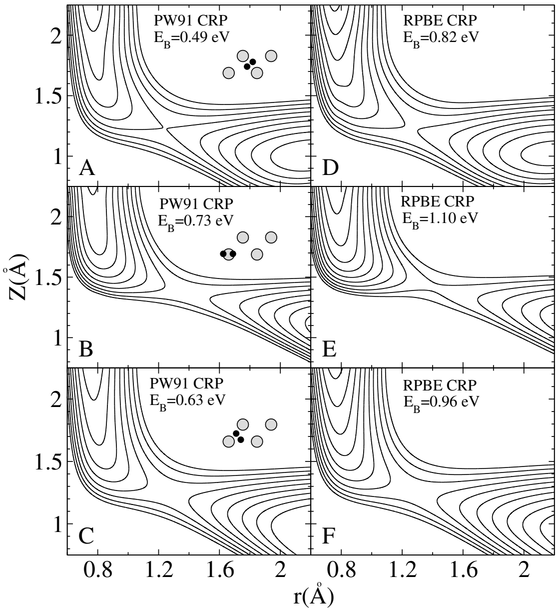

Figure 3.4.3: Figure extracted from Ref. [83]. 2D cuts through the the CRP-PW91-PES (**A**)-(**C**), and the CRP-RPBE-PES (**D**)-(**F**). (**A**, **B**) Bridge-to-hollow dissociation. (**B**, **E**) Top-to-bridge dissociation. (**C**, **F**) Dissociation above a site halfway between the top and the hcp sites with $\phi = 120^o$. The spacing between the contour levels is 0.1 eV.

Our analysis also allow us to explain the differences between computed rovibrational inelastic and elastic scattering probabilities for PW91-PES and RPBE-PES shown in section 3.3. Fig. 3.3.6 shows that PW91-PES calculations trend to yield higher vibrational deexcitation probabilities than RPBE-PES for every incidence energy. In fact, RPBE-PES calculations do not yield any vibrational inelastic scattering. Reaction barriers predicted by PW91-PES are systematically lower than those predicted by RPBE-PES[83] (see also Fig. 3.4.3). Therefore, the classical turning points in the former case are expected to be distributed at lower Z_{scat} values than those from the later one, i.e. for the PW91-PES the molecules are able to sample closer zones on the surface. Fig. 3.4.4 corroborates this statement. Trajectories moving along the RPBE-PES are scattered 0.5 $\sim$ 1 Å farther away than trajectories moving across the PW91-PES. Thus, they cannot reach zones with high V-T coupling, and vibrational deexcitation is not expected. At that point, we have to remark that the Z-distribution of classical turning points calculated using the RPBE-PES do not present two peaks as in the case of PW91 calculations, not even at 230 meV of incidence energy. Hence, a prominent role of scattering over top-site is not expected in the former case. This can be seen from Fig. 3.4.5, where we have plotted $X_{cm}Y_{cm}$-distribution of $H_2(v_i = 1, J_i = 1)$/Cu(111) (panels **A**, **B**) and $D_2(v_i = 1, J_i = 2)$/Cu(111) (panels **C**, **D**) classical turning points for PW91-PES (panels **A**, **C**) and RPBE-PES (panels **B**, **D**) at E_i=230 meV. Fig. 3.4.5 not only shows that RPBE-PES classical turning points (panels **B**, **D**) are not preferentially distributed close to the top-site for either isotopes, but that they are concentrated near to the bridge-site. This means that the probability of a given molecule (H_2 or D_2) to be scattered from a RPBE-PES top-site is much lower that being scattered from a bridge-site. In the case of PW91 classical turning points, Fig. 3.4.5 (panels **A**, **C**) shows the contrary scheme: top-site scattering is clearly enhanced to the detriment of the bridge-site one for both isotopes.

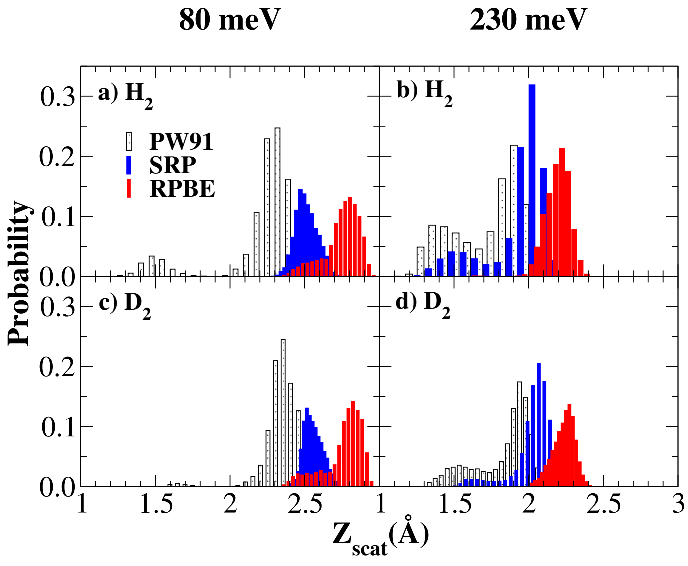

Figure 3.4.4: Distribution of classical turning points (Z_{scat}) of the molecules scattered from the SRP-PES (solid white bars), PW91-PES (solid blue bars) and RPBE-PES (solid red bars). (**a**) $H_2(v = 1, J = 1)$, E_i=80 meV; (**b**) $H_2(v = 1, J = 1)$, E_i=230 meV; (**c**) $D_2(v = 1, J = 2)$, E_i=80 meV; (**d**) $D_2(v = 1, J = 2)$, E_i=230 meV.

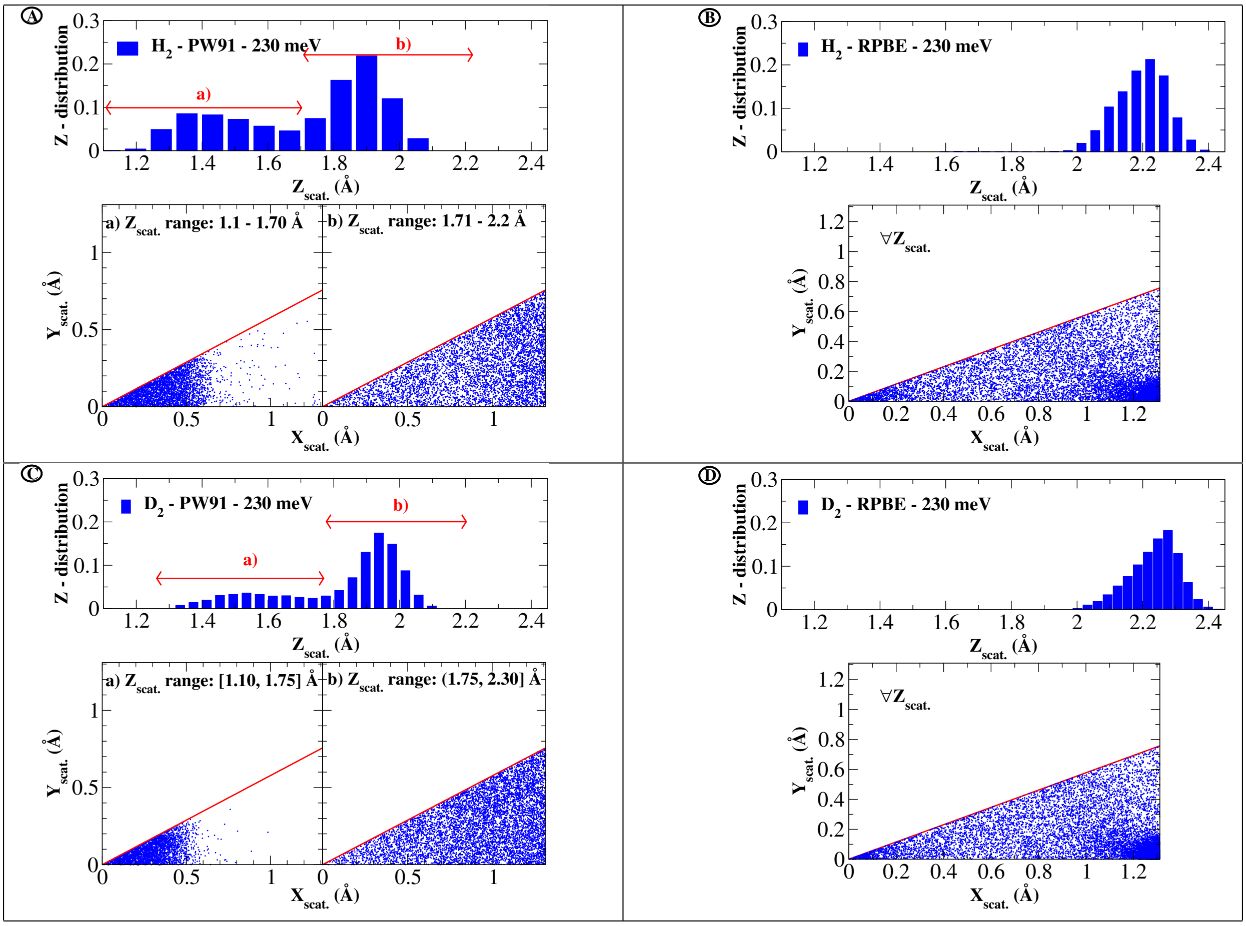

Figure 3.4.5: Similar study to Fig. 3.4.2, but for $H_2(v = 1, J = 1)$/Cu(111) PW91-PES (**A**), $H_2(v = 1, J = 1)$/Cu(111) RPBE-PES (**B**), $D_2(v = 1, J = 2)$/Cu(111) PW91-PES (**C**) and $D_2(v = 1, J = 2)$/Cu(111) RPBE-PES (**D**) at 230 meV of incidence energy.

In order to support the idea that the top-site scattering is enhancing the vibrational deexcitation process, we have also performed a classical turning point analysis only for those H_2 molecules that are being vibrationally deeexcited to the v=0 state (Fig. 3.4.6). In Fig. 3.4.6, we can see a dramatic decrease of the number of vibrationally deexcited molecules depending on the PES that was used for the calculations. The PW91-PES (panel **A**) presents the major ratio of deeexcited H_2molecules, followed by the SRP-PES (panel **B**) and RPBE-PES (panel **C**), where finally, we cannot find any deexcited molecule. This behavior is related with the barrier heights predicted by these PESs and it has been already explained above. What is important on Fig. 3.4.6, is the distribution of the classical turning points: all the vibrationally deexcited H_2 molecules, if present, were scattered close to the top-site (panels **A**, **B**). This result reinforces our hypothesis that the higher vibrational deexcitation effectiveness found theoretically in H_2/Cu(111) is due to the higher number of incident H_2 molecules that are scattered over the top-site, close to the surface, compared to D_2. A similar figure to 3.4.6 cannot be done for D_2/Cu(111) because at 230 meV of incidence energy there is not any vibrational deexcitation phenomena for any DFT-PES used in this work.

Classical calculations can be also employed to analyze rotational distribution of scattered trajectories. In Fig. 3.4.7 we have plotted the distribution of classical turning points (Z_{scat}) as a function of θ, which is the angle between the rotational axis of the molecule and the XY-plane (see section 1.3.1), for H_2/Cu(111) using the 3 PES considered in this work (PW91, RPBE, SRP). From Fig. 3.4.7, we can see that molecules which are scattered closer to the surface (low z values) trend to have a rotational axis perpendicular to the XY-plane ($\theta \approx 90^o$). This way of rotating is known in the literature as the helicopter state ($|m_j| = J$), which

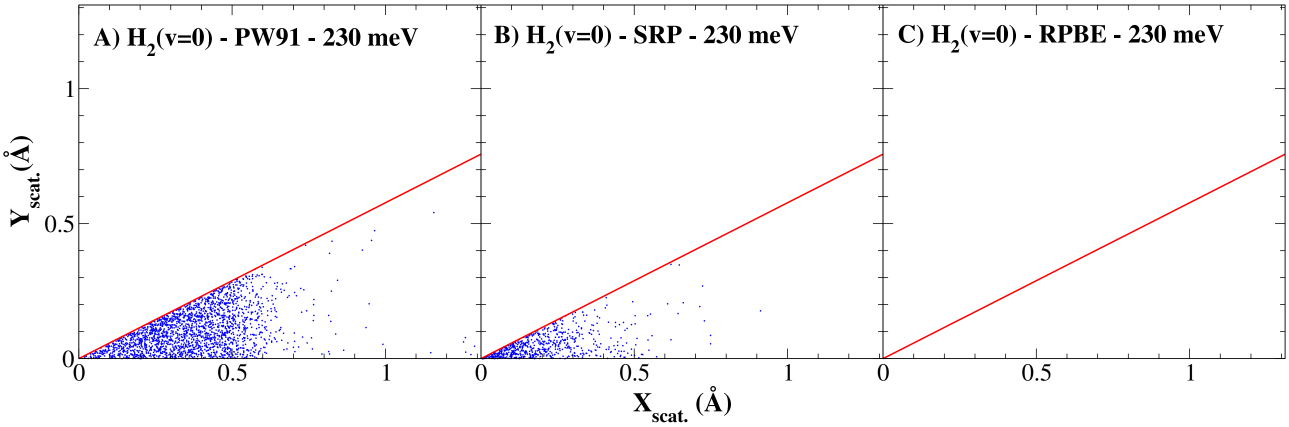

Figure 3.4.6: $X_{CM}Y_{CM}$-distribution of classical turning points for vibrationally deexcited scattered H_2(v=0)/Cu(111) molecules projected to the IWS cell. Panel **A**: PW91-PES calculations. Panel **B**: SRP-PES calculations. Panel **C**: RPBE-PES calculation.

is the one presenting the lowest reaction barriers on average, due to the lower repulsive steric interaction with the surface[25;76]. Thus, it is reasonable that molecules which are able to get closer to the surface are oriented this way (helicopter). From the comparison of Fig. 3.4.7 and Fig. 3.4.4 (panels **a**, **b**), focusing only in H_2 results, it is clear that the concentration of helicopter-scattered molecules close to the surface belong to the top-site scattering peak that appears in the Z-distribution analysis (Fig. 3.4.4). In those cases where this peak is low or is not present (RPBE-PES at E_i=80 meV and E_i=230 meV, or SRP-PES at E_i=80 meV) we can slightly see the described orientational preference. In Ref. [76], it was reported that there is a higher proportion of helicopter state reaction on top-site compared to other high-symmetry surface zones (bridge, hollow) for H_2/Cu(100) system. Our rotational analysis corroborates this phenomenon also for the Cu(111) surface.

Rotational analysis of classical turning points (Fig. 3.4.7) shows that the θ DOF plays an important role on the dynamics of $H_2(D_2)$/Cu(111) system. Only those molecules whose molecular axis is parallel or near parallel to the copper surface ($\theta \approx 90^o$) can reach close to the surface and be scattered from the top-site (see Fig. 3.4.7 and Fig. 3.4.4). As the molecules are initially random-oriented, these results suggest that molecules should be reoriented in their way in order to approach to the surface. In order to deeply study this phenomenon we have performed an exhaustive analysis of the H_2 classical trajectories as a function of Z, for 230 meV, where rotational effects should be more visible (see Fig. 3.4.7, panels **d**, **e**, **f**). From rotational distributions presented on Fig. 3.4.8 (**A** upper graphics), we can see that molecules which will be reflected close to the surface (solid red lines) are being slowly reoriented favoring helicopter states as they approach to the surface. It is also clear from the their XY-distribution (**C** bottom graphics), that these molecules are initially distributed close to the top site (red crosses, Z=5.5 panel) if we project them on the IWS-cell. The rest of the molecules, which are reflected farther from the surface (**A** upper graphics, dashed blue line), trend to lean their rotational axis up to approximately 30^0(150^o is equivalent by symmetry) from the XY plane when they are 2.5 far from the surface. Regarding their XY-distribution (Fig. 3.4.8, **C** graphics), they do not present any initial XY-position preference (blue crosses, Z=5.5). These results manifest the importance of letting $H_2(D_2)$ molecules rotate, i.e. the need for a multidimensional description of the system. The molecular reorientation minimizes the repulsive interaction with the surface, which allows the molecules to sample deeper zones of the PES. This phenomenon cannot be simulated by low dimensional models. Thus, our analysis allows us to understand why Luntz *et al.*[80] could not reproduce the isotope effect seen in the experiments[40;41] using the BOSS model. In their simulations, in addition to the lack of the top-site

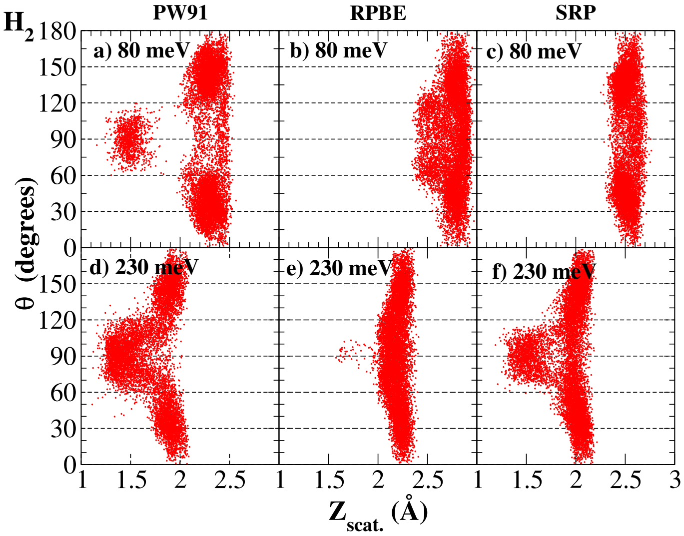

Figure 3.4.7: Distribution of classical turning points of the $H_2(v = 1, J = 1)$ molecules scattered from the PW91-PES (**a**, **d**), RPBE-PES (**b**, **e**) and SRP-PES (**c**, **f**) as a function of the angle formed between the rotational axis and the XY-plane (θ), and the distance to the surface (z_{scat}). (**a**) PW91-PES, E_i=80 meV. (**b**) RPBE-PES, E_i=80 meV. (**c**) SRP-PES, E_i=80 meV. (**d**) PW91-PES, E_i=230 meV. (**e**) RPBE-PES, E_i=230 meV. (**f**) SRP-PES, E_i=230 meV.

sampling, the scattered $H_2(D_2)$ molecules experimented higher average reaction barriers due to the lack of reorientation and were reflected farther from the surface, where V-T energy transfer is not efficient.

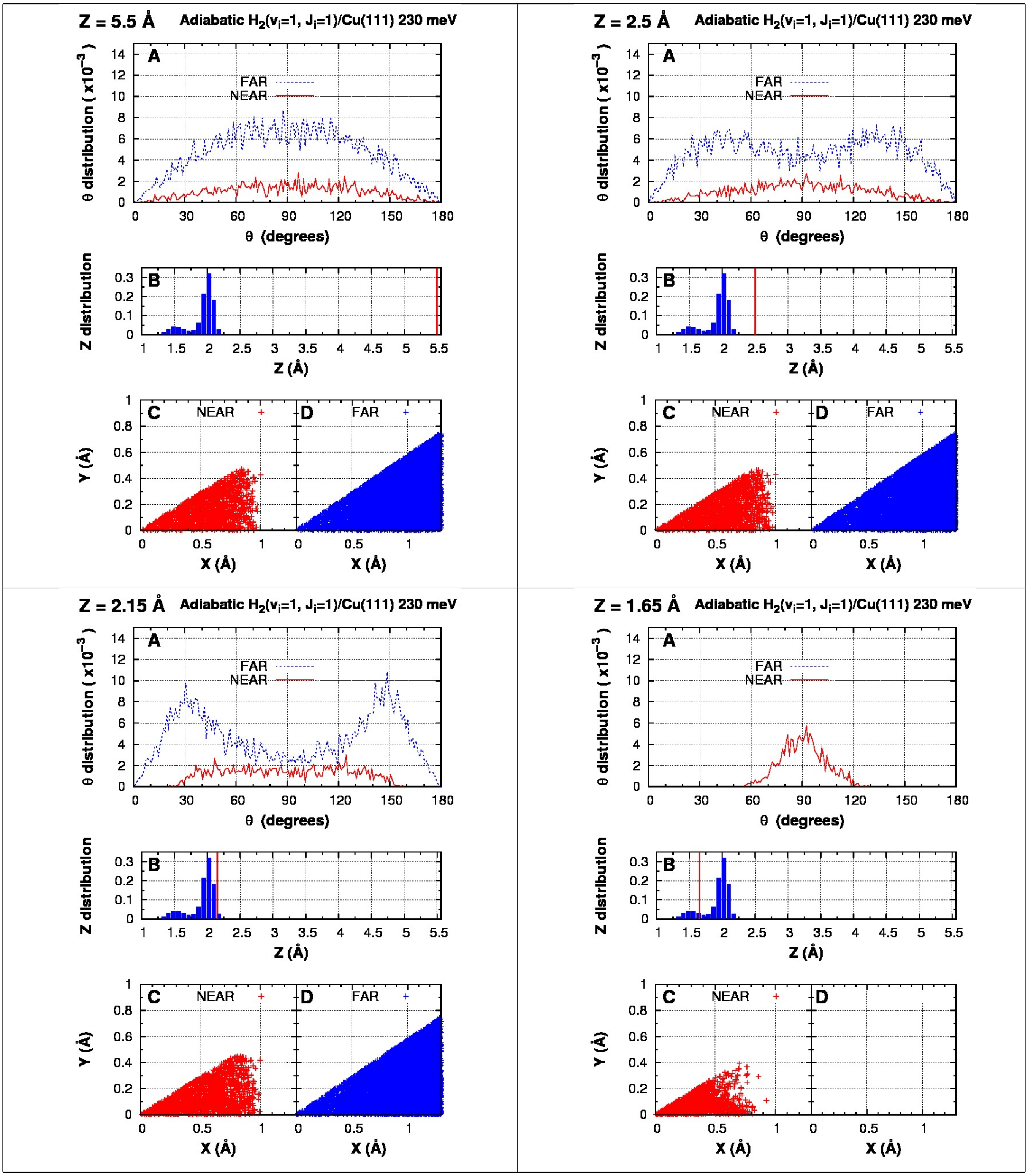

Figure 3.4.8: For each panel: (**A**) θ-distribution of scattered molecules that will reach closer to the surface (solid red line) and those that will be scattered farther (dashed blue line); (**B**) Z_{scat}-distribution of classical turning points (same as Fig. 3.4.1 panel **b**), the red line indicates the distance between incident molecules and the surface; (**C**) XY-distribution for scattered molecules that will reach closer zones to the surface (red points); (**D**) molecules that will be scattered farther. Top left panel: analysis for $H_2(v = 1, J = 1)$, $E_i = 230$ meV, Z=5.5 . Top right panel: analysis for $H_2(v = 1, J = 1)$, $E_i = 230$ meV, Z=2.5 . Bottom left panel: analysis for $H_2(v = 1, J = 1)$, $E_i = 230$ meV, Z=2.15 . Bottom right panel: analysis for $H_2(v = 1, J = 1)$, $E_i = 230$ meV, Z=1.65 .

SECTION: 3.5

Conclusions

We have performed adiabatic and non-adiabatic six-dimensional (6D) quasi-classical (QC) dynamics calculations of vibrational survival and the rotational excitation (and deexcitation) probabilities for H_2 (v_i =1, J_i =1) and D_2 (v_i =1, J_i =2) scattering from Cu(111). The accuracy of our QC calculations have been tested via a comparison with adiabatic quantum (Q) dynamics, that shows a qualitative good agreement between both Q and QC adiabatic results. We have shown that both 6D adiabatic and non-adiabatic calculations reproduce qualitatively the experimental isotope effect reported in Refs. [40;41] for the Cu(100) surface, according to which vibrational survival probabilities decrease with collision energy, the decrease being more pronounced for H_2 than for D_2. Our non-adiabatic calculations slightly change quantitatively the results obtained with the adiabatic model, therefore, our work support the idea that the loss of energy to electron-hole (e-h) pair excitations do no play a major role in the vibrational deexcitation of H_2 and D_2 scattering from Cu(111).

Taking advantage of our classical trajectories study, we have shown that molecules which get closer to the surface, scattered near the top-site, are responsible for vibrational deexcitation scattering. For these molecules, the high curvature of the reaction path in front of the barrier enhances the energy transfer from vibration to translation, favoring vibrationally inelastic processes. We have also shown that the probability for a molecule to approach the top-site is higher for H_2 than for D_2, which explains the isotopic effect found in the experiment.

Now the question is: why do more H_2 molecules hit to top site? This phenomenon is linked to vibrational softening, i.e., to the adiabatic energy transfer from the vibration to the translation mode. Vibrational energies of H_2 are 1.4 times larger then vibrational energies of D_2, thus the energy transfer is expected to be higher for H_2 (more energy available) than for D_2, i.e., H_2 molecules may have more energy to get closer to the barriers than D_2. This seems to be the reason why on average more H_2 molecules are scattered from the top site.

Results presented in this work also emphasize the importance of carring out high dimensional dynamics calculations, i.e. including at least all the molecular degrees of freedom (DOF), to understand the underlying physics behind $H_2(D_2)$/Cu interaction. Low dimensional calculations that only consider the reaction path containing the lowest energy barrier cannot describe a process that occurs in any other site, as shown in our analysis.

APPENDIX A

Incremented friction coefficients study

In order to assure that the influence of non-adiabatic e-h pair excitation processes introduced in the simulations within the LDFA is not very sensible to the way the friction coefficients are defined, we have carried out some calculations with unphysical high friction coefficients. These new coefficients are ten times higher than the ones calculated in Ref. [74], which are the same that we have used in section 3.3. With this study, we want to reinforce the idea that the LDAF is not introducing any artifact in our calculations and that we should lead to the same conclusions even with a different definition of the friction coefficients (see sections 3.5 and 2.4).

From Figs. A.1.1, A.2.1 and A.3.1 we can see that the elastic-scattering channels H_2(v=1, J=1)→(v=1, J=1) and D_2(v=1, J=2)→(v=1, J=2) slightly change from the adiabatic picture to the augmented friction coefficients study. The vibrational deexcitation channels H_2(v=1, J=1)→(v=0, J=1) and D_2(v=1, J=2)→(v=0, J=2) are clearly enhanced in the non-adiabatic calculations. The rotational excitation probabilities H_2(v=1, J=1)→(v=1, J=3) and D_2(v=1, J=2)→(v=1, J=4) decrease in the non-adiabatic picture respect to the adiabatic calculations. It is also evident that augmented non-adiabatic calculations disfavor dissociative adsorption probabilities as it could be expected (the dissipative force extracts energy from the molecular DOFs and the molecules cannot overcome the reaction barriers). We can see these tendencies no matter the PES we have used to run the dynamics: the PW91, the RPBE or the SRP one.

What we have to keep in mind from this study is that even using unphysical augmented friction coefficients, the global vibrational survival probabilities, i.e. H_2(v=1, J=1)→(v=1, ΣJ) and D_2(v=1, J=2)→(v=1, ΣJ), and the elastic scattering probabilities do not change qualitatively respect to the adiabatic calculations (which are the main properties where we can see the isotope effect). It is only changing the weight of the final rovibrational channels. This supports two main ideas:

- Non-adiabatic effects do not play a major role in the isotope effect found in the experiment.
- The conclusions obtained from the comparison of non-adiabatic and adiabatic calculations are not an artifact of the LDFA model.

SECTION: A.1

Rovibrational channels: PW91-PES

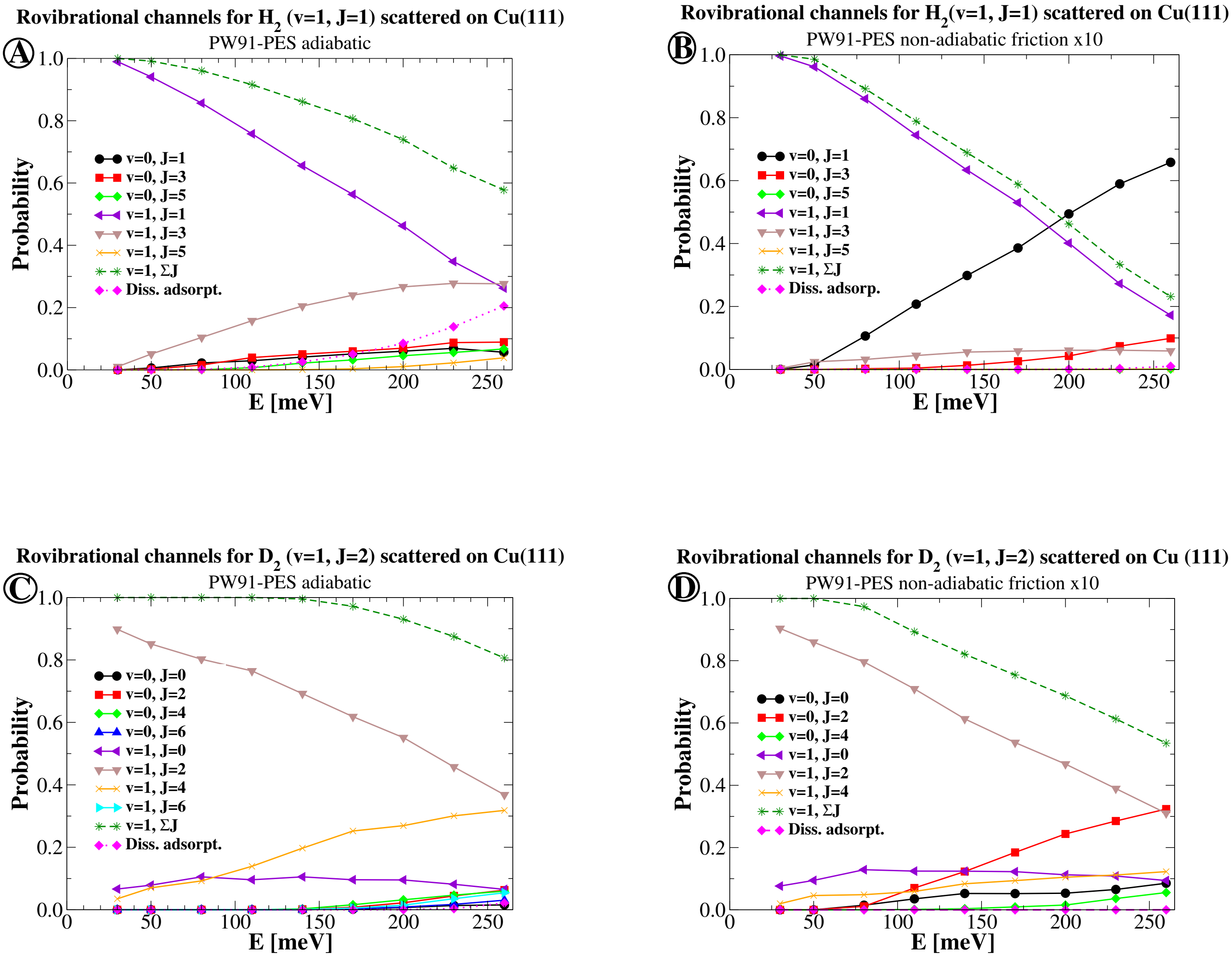

Figure A.1.1: H_2(v=1, J=1)/Cu(111) (**A**, **B**) and D_2(v=1, J=2)/Cu(111) (**C**, **D**) rovibrational elastic and inelastic probabilities as a function of incidence energy calculated with the PW91-PES. For each panel: (**A**, **C**) adiabatic calculations; (**B**, **D**) non-adiabatic calculations with augmented friction coefficients.

SECTION: A.2

Rovibrational channels: RPBE-PES

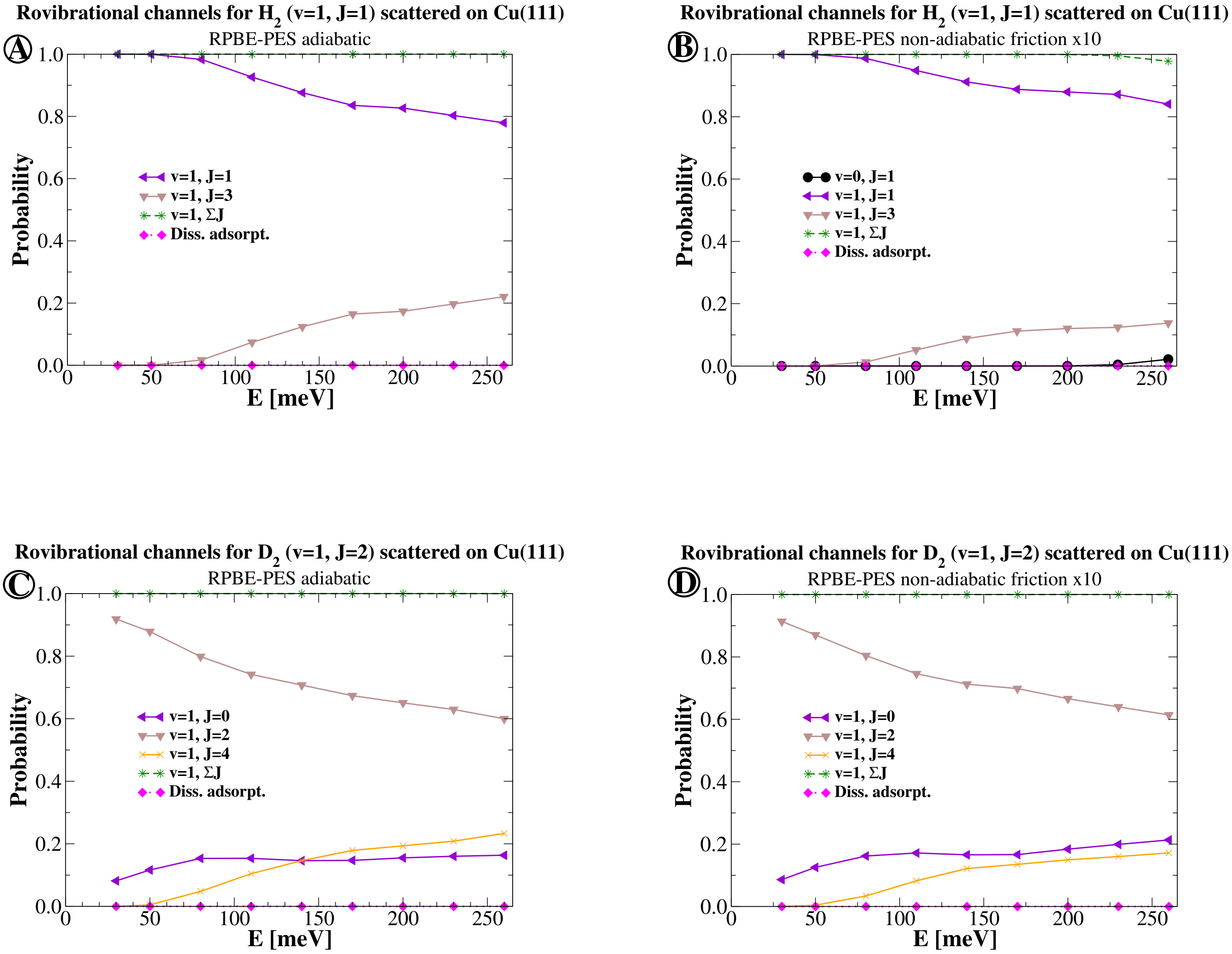

Figure A.2.1: H_2(v=1, J=1)/Cu(111) (**A**, **B**) and D_2(v=1, J=2)/Cu(111) (**C**, **D**) rovibrational elastic and inelastic probabilities as a function of incidence energy calculated with the RPBE-PES. For each panel: (**A**, **C**) adiabatic calculations; (**B**, **D**) non-adiabatic calculations with augmented friction coefficients.

SECTION: A.3

Rovibrational channels: SRP-PES

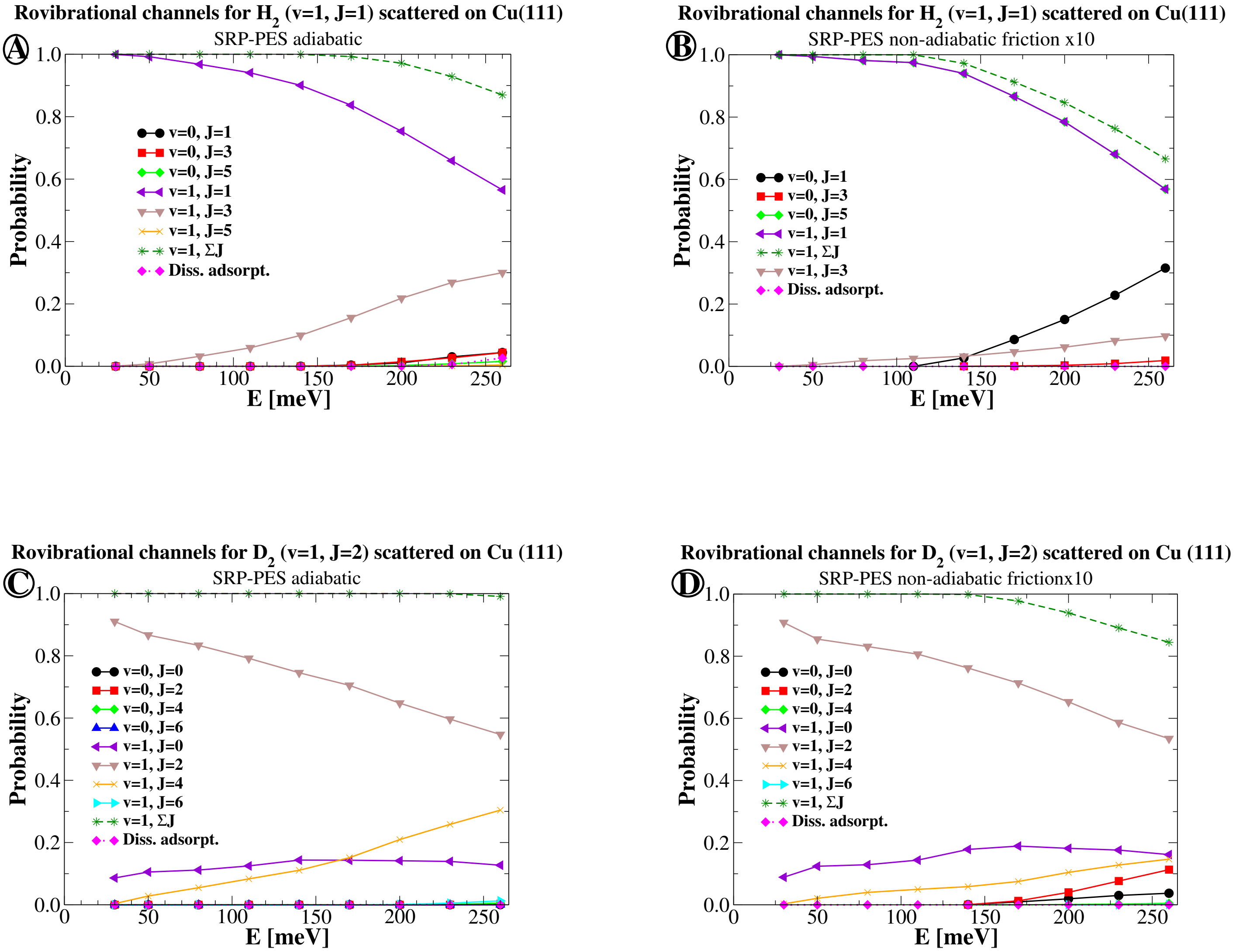

Figure A.3.1: H_2(v=1, J=1)/Cu(111) (**A**, **B**) and D_2(v=1, J=2)/Cu(111) (**C**, **D**) rovibrational elastic and inelastic probabilities as a function of incidence energy calculated with the SRP-PES. For each panel: (**A**, **C**) adiabatic calculations; (**B**, **D**) non-adiabatic calculations with augmented friction coefficients.

APPENDIX B

Output from this work

- **Article:** A. S. Muzas, J. I. Juaristi, M. Alducin, R. Díez Muiño, G. J. Kroes and C. Díaz. "*Vibrational deexcitation and rotational excitation of H_2 and D_2 scattered from Cu(111): Adiabatic versus non-adiabatic dynamics*", Journal of chemical physics (submitted).

……

- **Presentation:** *"Vibrational deexcitation and rotational excitation of H2 and D2 upon scattering from Cu(111): Adiabatic versus non-adiabatic dynamics"*. Department seminar for the Theoretical Chemistry group in Leiden Institute of Chemistry (Faculty of Science).

Bibliography

[1] Ya-Huei (Cathy) Chin, Cornelius Buda, Matthew Neurock, and Enrique Iglesia. "Reactivity of chemisorbed oxygen atoms and their catalytic consequences during CH_4-O-2 catalysis on supported Pt clusters". *Journal Of The American Chemical Society*, 133(40):15958–15978, OCT 12 2011.

[2] Laura S. Sremaniak and Jerry L. Whitten. "Theoretical treatment of excited electronic states of adsorbates on metals: Electron attachment to CO2 adsorbed on Pt(111)". *Surface Science*, 601:3755–3759, 2007.

[3] Stefan Vajda, Michael J. Pellin, Jeffrey P. Greeley, Christopher L. Marshall, Larry A. Curtiss, Gregory A. Ballentine, Jeffrey W. Elam, Stephanie Catillon-Mucherie, Paul C. Redfern, Faisal Mehmood, and Peter Zapol. "Subnanometre platinum clusters as highly active and selective catalysts for the oxidative dehydrogenation of propane". *Nature Materials*, 8(3):213–216, MAR 2009.

[4] H. Winter and A. Schueller. "Fast atom diffraction during grazing scattering from surfaces". *Progress In Surface Science*, 86(9-10):169–221, SEP-OCT 2011.

[5] B. Bogdanovic and M. Schwickardi. "Ti-doped alkali metal aluminium hydrides as potential novel reversible hydrogen storage materials". *Journal Of Alloys And Compounds*, 253:1–9, 1997.

[6] W. Lohstroh and M. Fichtner. "Rate limiting steps of the phase transformations in Ti-doped NaAlH4 investigated by isotope exchange". *Physical Review B*, 75(18), MAY 2007.

[7] Roberto Otero, José María Gallego, Amadeo L. Vázquez de Parga, Nazario Martín, and Rodolfo Miranda. "Molecular self-assembly at solid surfaces". *Advanced Materials*, 23(44, SI):5148–5176, NOV 23 2011.

[8] G. Ertl. "Primary steps in catalytic synthesis of ammonia". *Journal Of Vacuum Science & Technology A-vacuum Surfaces And Films*, 1(2):1247–1253, 1983.

[9] S Holloway and N V Richardson. *"Handbook of Surface Science"*, volume 3. North-Holland, 2008.

[10] G.R. Darling and S. Holloway. "Dissociation thresholds and the vibrational-excitation process in the scattering of H_2". *Surface Science*, 307:153–158, 1994.

[11] Chien-fan Yu, K.B. Whaley, C.S. Hogg, and S.J. Sibener. "Investigation of the spatially isotropic component of the laterally averaged molecular hydrogen/Ag(111) physisorption potential". *Journal of Chemical Physics*, 83:4217–34, 15 Oct. 1985.

[12] MJ Murphy and A Hodgson. "Role of surface thermal motion in the dissociative chemisorption and recombinative desorption of D_2 on Ag(111)". *Physical Review Letters*, 78(23):4458–4461, JUN 9 1997.

[13] G Kresse. "Dissociation and sticking of H_2 On the Ni(111), (100), and (110) substrate". *Physical Review B*, 62(12):8295–8305, SEP 15 2000.

[14] A. Gross, S. Wilke, and M. Scheffler. "6-dimensional quantum dynamics of adsorption and desorption of H_2 at Pd(100) - steering and steric effects". *Physical Review Letters*, 75(14):2718–2721, OCT 2 1995.

[15] Cristina Díaz. *"Difusión molecular por superficies metalicas: H_2/Pd(111 y H_2/Pd(110)"*. PhD thesis, Universidad Autónoma de Madrid, 2004.

[16] S Wilke and M Scheffler. "Potential-energy surface for H_2 dissociation over Pd(100)". *Physical Review B*, 53(8):4926–4932, FEB 15 1996.

[17] A Dianat and A Gross. "High-dimensional quantum dynamical study of the dissociation of H_2 on Pd(110)". *Journal Of Chemical Physics*, 120(11):5339–5346, MAR 15 2004.

[18] C Crespos, HF Busnengo, W Dong, and A Salin. "Analysis of H_2 dissociation dynamics on the Pd(111) surface". *Journal Of Chemical Physics*, 114(24):10954–10962, JUN 22 2001.

[19] J.A. White, D.M. Bird, and M.C. Payne. "Dissociation of H_2 on W(100)". *Physical Review B*, 53(3):1667–1674, JAN 15 1996.

[20] K.D. Rendulic, G. Anger, and A. Winkler. "Wide-range nozzle beam adsorption data for the systems H_2 nickel and H_2/pd(100)". *Surface Science*, 208(3):404–424, FEB 1989.

[21] B. Jackson and H. Metiu. "The dynamics of H_2 dissociation on Ni(100) - a quantum-mechanical study of a restricted two-dimensional model". *Journal Of Chemical Physics*, 86(2):1026–1035, JAN 15 1987.

[22] M.R. Hand and S. Holloway. "A theoretical-study of the dissociation of H_2/Cu". *Journal Of Chemical Physics*, 91(11):7209–7219, DEC 1 1989.

[23] J. Sheng and J.Z.H. Zhang. "Dissociative chemisorption of H_2 on Ni surface - time-dependent quantum dynamics calculation and comparison with experiment". *Journal Of Chemical Physics*, 96(5):3866–3874, MAR 1 1992.

[24] R.C. Mowrey. "Dissociative adsorption of H_2 using the close-coupling wave-packet method". *Journal of Chemical Physics*, 99(9):7049–7055, NOV 1 1993.

[25] G.R. Darling and S. Holloway. "Angular and vibrational effects in the sticking and scattering of H_2". *Journal Of Chemical Physics*, 97(7):5182–5192, OCT 1 1992.

[26] Jiqiong Dai and J.Z.H. Zhang. "Steric effect in dissociative chemisorption of hydrogen on Cu". *Surface Science*, 319:193–8, 1 Nov. 1994.

[27] A. Gross. "The role of lateral surface corrugation for the quantum dynamics of dissociative adsorption and associative desorption". *Journal Of Chemical Physics*, 102(12):5045–5058, MAR 22 1995.

[28] G.R. Darling and S. Holloway. "Rotational motion and the dissociation of H_2 on Cu(111)". *Journal Of Chemical Physics*, 101(4):3268–3281, AUG 15 1994.

[29] J.Q. Dai and J.Z.H. Zhang. "Quantum adsorption dynamics of a diatomic molecule on surface - 4-dimensional fixed-site model for H_2 on Cu(111)". *Journal Of Chemical Physics*, 102(15):6280–6289, APR 15 1995.

[30] G.J. Kroes, G. Wiesenekker, E.J. Baerends, and R.C. Mowrey. "Competition between vibrational excitation and dissociation in collisions of H_2 with Cu(100)". *Physical Review B*, 53(15):10397–10401, APR 15 1996.

[31] J.Q. Dai and J.C. Light. "Six dimensional quantum dynamics study for dissociative adsorption of H_2 on Cu(111) surface". *Journal Of Chemical Physics*, 107(5):1676–1679, AUG 1 1997.

[32] G.J. Kroes, E.J. Baerends, and R.C. Mowrey. "Six-dimensional quantum dynamics of dissociative chemisorption of H_2 on Cu(100)". *Journal Of Chemical Physics*, 107(8):3309–3323, AUG 22 1997.

[33] G.J. Kroes, E.J. Baerends, and R.C. Mowrey. "Six-dimensional quantum dynamics of dissociative chemisorption of (v = 0,j = 0) H_2 on Cu(100)". *Physical Review Letters*, 81(21):4781, NOV 23 1998.

[34] G.J. Kroes. "Six-dimensional quantum dynamics of dissociative chemisorption of H_2 on metal surfaces". *Progress In Surface Science*, 60(1-4):1–85, JAN-FEB 1999.

[35] C. Engdahl and U. Nielsen. "Hydrogen dissociation on copper - importance of dimensionality in calculations of the sticking coefficient". *Journal Of Chemical Physics*, 98(5):4223–4233, MAR 1 1993.

[36] C.M. Wei, A. Gross, and M. Scheffler. "Ab initio calculation of the potential energy surface for the dissociation of H_2 on the sulfur-covered Pd(100) surface". *Physical Review B*, 57(24):15572–15584, JUN 15 1998.

[37] H.F. Busnengo, .C Crespos, W. Dong, J.C. Rayez, and A. Salin. "Classical dynamics of dissociative adsorption for a nonactivated system: The role of zero point energy". *Journal Of Chemical Physics*, 116(20):9005–9013, MAY 22 2002.

[38] H A Michelsen, C T Rettner, and D J Auerbach. *"Surface Reactions"*, volume 1. Springer, Series in Surface Science 34, 1993.

[39] C.T. Rettner, H.A. Michelsen, and D.J. Auerbach. "Determination of quantum-state-specific gas-surface energy-transfer and adsorption probabilities as a function of kinetic-energy". *Chemical Physics*, 175(1):157–169, SEP 1 1993.

[40] E. Watts and G.O. Sitz. "State-to-state scattering in a reactive system: H-2(v=1,J=1) from Cu(100)". *Journal Of Chemical Physics*, 114(9):4171–4179, MAR 1 2001.

[41] L.C. Shackman and G.O. Sitz. "State-to-state scattering of D_2 from Cu(100) and Pd(111)". *Journal Of Chemical Physics*, 123(6), AUG 8 2005.

[42] H.A. Michelsen, C.T. Rettner, D.J. Auerbach, and R.N. Zare. "Effect of rotation on the translational and vibrational-energy dependence of the dissociative adsorption of D_2 on Cu(111)". *Journal Of Chemical Physics*, 98(10):8294–8307, MAY 15 1993.

[43] W. Allison and B. Feuerbacher. "Rotationally Inelastic Molecule-surface Scattering". *Physical Review Letters*, 45(25):2040–2043, 1980.

[44] D. Cvetko, A. Morgante, A. Santaniello, and F. Tommasini. "Deuterium scattering from Rh(110) surface". *Journal Of Chemical Physics*, 104(19):7778–7783, MAY 15 1996.

[45] M. Gostein, E. Watts, and G. O. Sitz. "Vibrational relaxation of H_2 (v=1, J=1) on Pd(111)". *Physical Review Letters*, 79:2891–2894, Oct 1997.

[46] M. Gostein, H. Parhikhteh, and G.O. Sitz. "Survival probability of H_2 (v=1, j=1) scattered from Cu(110)". *Physical Review Letters*, 75(2):342–345, JUL 10 1995.

[47] C.T. Rettner, D.J. Auerbach, and H.A. Michelsen. "Observation of direct vibrational-excitation in collisions of H_2 and D_2 with a Cu(111) surface". *Physical Review Letters*, 68(16):2547–2550, APR 20 1992.

[48] D.A. King and M.G. Wells. "Reaction-mechanism in chemisorption kinetics - nitrogen on (100) plane of tungsten". *Proceedings Of The Royal Society Of London Series A-mathematical And Physical Sciences*, 339(1617):245–269, 1974.

[49] M. Balooch, M.J. Cardillo, D.R. Miller, and R.E. Stickney. "Molecular-beam study of apparent activation barrier associated with adsorption and desorption of hydrogen on copper". *Surface Science*, 46(2):358–392, 1974.

[50] B.E. Hayden and C.L.A. Lamont. "Coupled translational-vibrational activation in dissociative hydrogen adsorption on Cu(110)". *Physical Review Letters*, 63(17):1823–1825, OCT 23 1989.

[51] H.A. Michelsen, C.T. Rettner, and D.J. Auerbach. "State-specific dynamics of D_2 desorption from Cu(111) - the role of molecular rotational motion in activated adsorption-desorption dynamics". *Physical Review Letters*, 69(18):2678–2681, NOV 2 1992.

[52] W. Van Willigen. *Physical Letters*, 28A:80, 1968.

[53] G.D Kubiak, G.O. Sitz, and R.N. Zare. "Recombinative desorption dynamics - molecular-hydrogen from Cu(110) and Cu(111)". *Journal Of Chemical Physics*, 83(5):2538–2551, 1985.

[54] C.T. Rettner, H.A. Michelsen, and D.J. Auerbach. "Quantum-state-specific dynamics of the dissociative adsorption and associative desorption of H_2 at a Cu(111) surface". *Journal Of Chemical Physics*, 102(11):4625–4641, MAR 15 1995.

[55] B.N.J. Persson and M. Persson. "Damping of vibrations in molecules adsorbed on a metal-surface". *Surface Science*, 97(2-3):609–624, 1980.

[56] B.N.J. Persson and M. Persson. "Vibrational lifetime for CO adsorbed on Cu(100)". *Solid State Communications*, 36(2):175–179, 1980.

[57] Y. Huang, A.M. Wodtke, H. Hou, C.T. Rettner, and D.J. Auerbach. "Observation of vibrational excitation and deexcitation for NO(v=2) scattering from Au(111): Evidence for electron-hole-pair mediated energy transfer". *Physical Review Letters*, 84(13):2985–2988, MAR 27 2000.

[58] Y.H. Huang, C.T. Rettner, D.J. Auerbach, and A.M. Wodtke. "Vibrational promotion of electron transfer". *Science*, 290(5489):111–114, OCT 6 2000.

[59] A. Gross and W. Brenig. "Adiabatic versus nonadiabatic effects in the vibrational-excitation in NO/Ag scattering". *Chemical Physics*, 177(2):497–508, NOV 15 1993.

[60] A. Gross and W. Brenig. "Vibrational-excitation of NO in NO/Ag scattering revisited". *Surface Science*, 289(3):335–339, JUN 1 1993.

[61] H. Nienhaus, H.S. Bergh, B. Gergen, A. Majumdar, W.H. Weinberg, and E.W. McFarland. "Electron-hole pair creation at Ag and Cu surfaces by adsorption of atomic hydrogen and deuterium". *Physical Review Letters*, 82(2):446–449, JAN 11 1999.

[62] Eckart Hasselbrink. "Non-adiabaticity in surface chemical reactions". *Surface Science*, 603(10-12):1564–1570, JUN 1 2009.

[63] D. Krix, R. Nuenthel, and H. Nienhaus. "Generation of hot charge carriers by adsorption of hydrogen and deuterium atoms on a silver surface". *Physical Review B*, 75(7), FEB 2007.

[64] L. Osterlund, I. Zoric, and B. Kasemo. "Dissociative sticking of O_2 on Al(111)". *Physical Review B*, 55(23):15452–15455, JUN 15 1997.

[65] M. Alducin, H.F. Busnengo, and R. Diez Muino. "Dissociative dynamics of spin-triplet and spin-singlet O-2 on Ag(100)". *Journal of Chemical Physics*, 129(22), DEC 14 2008.

[66] J. Behler, B. Delley, S. Lorenz, K. Reuter, and M. Scheffler. "Dissociation of O-2 at Al(111): the role of spin selection rules". *Physical Review Letters*, 94(3), JAN 28 2005.

[67] Neil Shenvi, Sharani Roy, Priya Parandekar, and John Tully. "Vibrational relaxation of NO on Au(111) via electron-hole pair generation". *Journal Of Chemical Physics*, 125(15), OCT 21 2006.

[68] Neil Shenvi, Sharani Roy, and John C. Tully. "Dynamical steering and electronic excitation in NO scattering from a gold surface". *Science*, 326(5954):829–832, NOV 6 2009.

[69] Serge Monturet and Peter Saalfrank. "Role of electronic friction during the scattering of vibrationally excited nitric oxide molecules from Au(111)". *Physical Review B*, 82(7), AUG 5 2010.

[70] L. Diekhoner, L. Hornekaer, H. Mortensen, E. Jensen, A. Baurichter, VV. Petrunin, and A.C. Luntz. "Indirect evidence for strong nonadiabatic coupling in N_2 associative desorption from and dissociative adsorption on Ru(0001)". *Journal Of Chemical Physics*, 117(10):5018–5030, SEP 8 2002.

[71] C. Díaz, J. K. Vincent, G. P. Krishnamohan, R. A. Olsen, G. J. Kroes, K. Honkala, and J. K. Norskov. "Reactive and nonreactive scattering of N_2 from Ru(0001): A six-dimensional adiabatic study". *Journal Of Chemical Physics*, 125(11), SEP 21 2006.

[72] P. Nieto, E. Pijper, D. Barredo, G. Laurent, R.A. Olsen, E.J. Baerends, G.J. Kroes, and D. Farias. "Reactive and nonreactive scattering of H_2 from a metal surface is electronically adiabatic". *Science*, 312(5770):86–89, APR 7 2006.

[73] K. R. Geethalakshmi, J. I. Juaristi, R. Díez Muiño, and M. Alducin. "Non-reactive scattering of N_2 from the W(110) surface studied with different exchange-correlation functionals". *Physical Chemistry Chemical Physics*, 13(10):4357–4364, 2011.

[74] J. I. Juaristi, M. Alducin, R. Díez Muiño, H. F. Busnengo, and A. Salin. "Role of electron-hole pair excitations in the dissociative adsorption of diatomic molecules on metal surfaces". *Physical Review Letters*, 100(11), MAR 21 2008.

[75] L. Martin-Gondre, M. Alducin, G. A. Bocan, R. Díez Muiño, and J. I. Juaristi. "Competition between electron and phonon excitations in the scattering of nitrogen atoms and molecules off tungsten and silver metal surfaces". *Physical Review Letters*, 108(13), MAR 26 2012.

[76] D.A. McCormack, G.J. Kroes, R.A. Olsen, J.A. Groeneveld, J.N.P. van Stralen, E.J. Baerends, and R.C. Mowrey. "Quantum dynamics of the dissociation of H-2 on Cu(100): Dependence of the site-reactivity on initial rovibrational state". *Faraday Discussions*, 117:109–132, 2000.

[77] G J. Kroes, E. Pijper, and A. Salin. "Dissociative chemisorption of H_2 on the Cu(110) surface: A quantum and quasiclassical dynamical study". *Journal Of Chemical Physics*, 127(16), OCT 28 2007.

[78] C. Díaz, E. Pijper, R. A. Olsen, H. F. Busnengo, D. J. Auerbach, and G. J. Kroes. "Chemically Accurate Simulation of a Prototypical Surface Reaction: H_2 Dissociation on Cu(111)". *Science*, 326(5954):832–834, NOV 6 2009.

[79] C. Díaz, R.A. Olsen, D.J. Auerbach, and G.J. Kroes. "Six-dimensional dynamics study of reactive and non reactive scattering of H_2 from Cu(111) using a chemically accurate potential energy surface". *Physical Chemistry Chemical Physics*, 12:6499–519, 28 June 2010.

[80] A.C. Luntz, M. Persson, and G.O. Sitz. "Theoretical evidence for nonadiabatic vibrational deexcitation in H-2(D-2) state-to-state scattering from Cu(100)". *Journal Of Chemical Physics*, 124(9), MAR 7 2006.

[81] J.P. Perdew, J.A. Chevary, S.H. Vosko, K.A. Jackson, M.R. Pederson, D.J. Singh, and C. Fiolhais. "Atoms, molecules, solids, and surfaces - applications of the generalized gradient approximation for exchange and correlation". *Physical Review B*, 46(11):6671–6687, SEP 15 1992.

[82] B. Hammer, L.B. Hansen, and J.K. Norskov. "Improved adsorption energetics within density-functional theory using revised Perdew-Burke-Ernzerhof functionals". *Physical Review B*, 59(11):7413–7421, MAR 15 1999.

[83] C. Díaz, R. A. Olsen, H. F. Busnengo, and G. J. Kroes. "Dynamics on Six-Dimensional Potential Energy Surfaces for H_2/Cu(111): Corrugation Reducing Procedure versus Modified Shepard Interpolation Method and PW91 versus RPBE". *Journal Of Physical Chemistry C*, 114(25):11192–11201, JUL 1 2010.

[84] H.A. Michelsen, C.T. Rettner, D.J. Auerbach, and R.N. Zare. "Effect of rotation on the translational and vibrational-energy dependence of the dissociative adsorption of D_2 on Cu(111)". *Journal Of Chemical Physics*, 98(10):8294–8307, MAY 15 1993.

[85] C Kittle. *"Introduction to Solid State Physics"*. 1971.

[86] http://dcwww.camp.dtu.dk/campos/dacapor.

[87] H.F. Busnengo, A. Salin, and W. Dong. "Representation of the 6D potential energy surface for a diatomic molecule near a solid surface". *Journal Of Chemical Physics*, 112(17):7641–7651, MAY 1 2000.

[88] J Stoer and R Burlisch. *"Introduction to Numerical Analysis"*. Springer, 1993.

[89] R.A. Leacock and P.W. Oconnor. "Action-variable theory and classical frequencies". *Journal Of Computational Physics*, 62(1):164–179, JAN 1986.

[90] J.A. Fleck, J.R. Morris, and M.D. Feit. "Time-dependent propagation of high-energy laser-beams through atmosphere". *Applied Physics*, 10(2):129–160, 1976.

[91] M.D. Feit, J.A. Fleck, and A. Steiger. "Solution of the Schrodinger-equation by a spectral method". *Journal Of Computational Physics*, 47(3):412–433, 1982.

[92] G.G. Balintkurti, R.N. Dixon, and C.C. Marston. "Grid methods for solving the schrodinger-equation and time-dependent quantum dynamics of molecular photofragmentation and reactive scattering processes". *International Reviews In Physical Chemistry*, 11(2):317–344, SEP 1992.

[93] R.C. Mowrey and G.J. Kroes. Application of an efficient asymptotic analysis method to molecule-surface scattering. *Journal Of Chemical Physics*, 103(3):1216–1225, JUL 15 1995.

[94] A. Vibok and G.G. Balintkurti. "Parametrization of complex absorbing potentials for time-dependent quantum dynamics". *Journal Of Physical Chemistry*, 96(22):8712–8719, OCT 29 1992.

[95] P.M. Echenique, R.M. Nieminen, and R.H. Ritchie. "Density functional calculation of stopping power of an electron-gas for slow ions". *Solid State Communications*, 37(10):779–781, 1981.

[96] M. Headgordon and J.C. Tully. "Molecular-dynamics with electronic frictions". *Journal Of Chemical Physics*, 103(23):10137–10145, DEC 15 1995.

[97] J.I. Juaristi, A. Arnau, P.M. Echenique, C. Auth, and H. Winter. "Charge state dependence of the energy loss of slow ions in metals". *Physical Review Letters*, 82(5):1048–1051, FEB 1 1999.

[98] R.D. Muiño and A. Salin. Energy and angular momentum transfer in the excitation of electron-hole pairs by slow dimers. *Physical Review B*, 62(8):5207–5215, AUG 15 2000.

[99] A. Salin, A. Arnau, P.M. Echenique, and E. Zaremba. "Dynamic nonlinear screening of slow ions in an electron gas". *Physical Review B*, 59(4):2537–2548, JAN 15 1999.

[100] M. Alducin, R. Díez Muiño, and J.I. Juaristi. "Energy dissipation channels in reactive and non-reactive scattering at surfaces". (to be published).

[101] Jennifer L. W. Siders and Greg O. Sitz. "Observation and characterization of direct inelastic and trapping-desorption channels in the scattering of N2 from Cu(110)". *Journal of Chemical Physics*, 101(7):6264, 1994.

[102] J.R. Trail, D.M. Bird, M. Persson, and S. Holloway. "Electron-hole pair creation by atoms incident on a metal surface". *Journal Of Chemical Physics*, 119(8):4539–4549, AUG 22 2003.

[103] Tapas Sahoo, Subhankar Sardar, Padmabati Mondal, Biplab Sarkar, and Satrajit Adhikari. "Effect of surface modes on the six-dimensional molecule-surface scattering dynamics of H_2-Cu(100) and D_2-Cu(111) systems". *Journal Of Physical Chemistry A*, 115(21):5256–5273, JUN 2 2011.

[104] Geert-Jan Kroes, Cristina Diaz, Ernst Pijper, Roar A. Olsen, and Daniel J. Auerbach. "Apparent failure of the Born-Oppenheimer static surface model for vibrational excitation of molecular hydrogen on copper". *Proceedings Of The National Academy Of Sciences Of The United States Of America*, 107(49):20881–20886, DEC 7 2010.

[105] Francesco Nattino, Cristina Díaz, Bret Jackson, and Geert-Jan Kroes. "Effect of surface motion on the rotational quadrupole alignment parameter of D_2 reacting on Cu(111)". *Physical Review Letters*, 108(23), JUN 8 2012.